Mammalian target of rapamycin and glycogen synthase kinase 3 differentially regulate lipopolysaccharide-induced interleukin-12 production in dendritic cells

Masashi Ohtani,[1,2] Shigenori Nagai,[1,2] Shuhei Kondo,[1] Shinta Mizuno,[1] Kozue Nakamura,[1] Masanobu Tanabe,[3] Tsutomu Takeuchi,[3] Satoshi Matsuda,[1,2] and Shigeo Koyasu[1,2]

[1]Department of Microbiology and Immunology, Keio University School of Medicine, Tokyo; [2]Core Research for Evolutional Science and Technology, Japan Science and Technology Agency, Saitama; and [3]Department of Tropical Medicine and Parasitology, Keio University School of Medicine, Tokyo, Japan

Phosphoinositide 3-kinase (PI3K) negatively regulates Toll-like receptor (TLR)–mediated interleukin-12 (IL-12) expression in dendritic cells (DCs). We show here that 2 signaling pathways downstream of PI3K, mammalian target of rapamycin (mTOR) and glycogen synthase kinase 3 (GSK3), differentially regulate the expression of IL-12 in lipopolysaccharide (LPS)–stimulated DCs. Rapamycin, an inhibitor of mTOR, enhanced IL-12 production in LPS-stimulated DCs, whereas the activation of mTOR by lentivirus-mediated transduction of a constitutively active form of Rheb suppressed the production of IL-12. The inhibition of protein secretion or deletion of IL-10 cancelled the effect of rapamycin, indicating that mTOR regulates IL-12 expression through an autocrine action of IL-10. In contrast, GSK3 positively regulates IL-12 production through an IL-10–independent pathway. Rapamycin-treated DCs enhanced Th1 induction in vitro compared with untreated DCs. LiCl, an inhibitor of GSK3, suppressed a Th1 response on *Leishmania major* infection in vivo. These results suggest that mTOR and GSK3 pathways regulate the Th1/Th2 balance though the regulation of IL-12 expression in DCs. The signaling pathway downstream of PI3K would be a good target to modulate the Th1/Th2 balance in immune responses in vivo. (Blood. 2008; 112:635-643)

Introduction

Dendritic cells (DCs) recognize pathogens via pattern-recognition receptors, such as Toll-like receptors (TLRs), nucleotide-binding oligomerization domain (NOD)-like receptors, and retinoic acid inducible gene-1 (RIG-I)-like receptors, produce various cytokines, including interleukin-12 (IL-12), and thus activate the innate immune system, which in turn leads to the induction of adaptive immunity.[1-5] Bioactive IL-12 is composed of p40 and p35 subunits and functions as a crucial inducer of Th1 responses. IL-12 is typically produced by antigen-presenting cells such as DCs and monocytes-macrophages and plays an important role in infection and tumor immunity.[1-5] Because the overproduction of IL-12 gives rise to strong cell-mediated immunity and organ-specific autoimmune diseases via exaggerated Th1 cell differentiation, it is critical that IL-12 levels be tightly controlled.[5]

Phosphoinositide 3-kinases (PI3Ks) are lipid kinases playing important roles in various signal transduction pathways.[6] PI3K family members are classified into 4 subgroups according to their structure and substrate specificity. Among them, class IA heterodimeric PI3Ks are involved in receptor-mediated signaling pathways in the immune system.[6,7] Phosphatidylinositol-(3,4)bisphosphate and phosphatidylinositol(3,4,5)trisphosphate produced by class IA PI3Ks recruit specific signaling proteins containing a pleckstrin homology domain to the plasma membrane. These proteins include Akt and phosphoinositide-dependent kinase 1 and are involved in a wide range of cellular responses, such as cell growth, survival, and cytokine production.[6,7] PI3K signaling pathways are counteracted by phosphatase and tensin homologue deleted on chromosome 10 (PTEN), a 3-phosphoinositide–specific lipid phosphatase.[6]

We have previously demonstrated that PI3K negatively regulates IL-12 production in DCs stimulated with TLR ligands.[8,9] An enhanced Th1 response was observed on *Leishmania major* infection,[8] and an impaired Th2 response was observed on *Strongyloides venezuelensis* infection[10] in mice deficient for p85α, a major regulatory subunit of class IA PI3K, indicating that PI3K plays a key role in the regulation of Th1/ Th2 balance in vivo. Although several reports confirmed the negative feedback regulation of IL-12 production by PI3K on TLR stimulation,[11-13] the molecular mechanism(s) remains controversial.

One downstream substrate of PI3K pathways is a Ser/Thr protein kinase named "mammalian target of rapamycin" (mTOR), which regulates cell growth and protein synthesis by activating p70 S6 kinase (p70S6K) and by inhibiting eukaryotic initiation factor 4E-binding protein 1 (4E-BP1).[14] There are 2 functionally distinct mTOR complexes, mTORC1 and mTORC2, and only mTORC1 acts downstream of the PI3K-Akt-tuberous sclerosis complex 2 (TSC2)–Rheb signaling pathway to phosphorylate p70S6K and 4E-BP1 in a rapamycin-sensitive fashion[14] (Figure 1A). Although the mTOR pathway is activated in response to not only growth factors but also environmental stresses such as hypoxia,[14] the TLR-triggered mTOR function is poorly understood. In the present study, we show that mTOR negatively regulates IL-12 production through the production of IL-10 in DCs. We further demonstrate that glycogen synthase kinase 3 (GSK3), another downstream target of PI3K pathways, is also involved in the PI3K-mediated regulation of IL-12 production in a manner distinct from that of mTOR. We also provide evidence that the inhibition of mTOR and

Submitted February 1, 2008; accepted April 9, 2008. Prepublished online as *Blood* First Edition paper, May 20, 2008; DOI 10.1182/blood-2008-02-137430.

The online version of this article contains a data supplement.

The publication costs of this article were defrayed in part by page charge payment. Therefore, and solely to indicate this fact, this article is hereby marked "advertisement" in accordance with 18 USC section 1734.

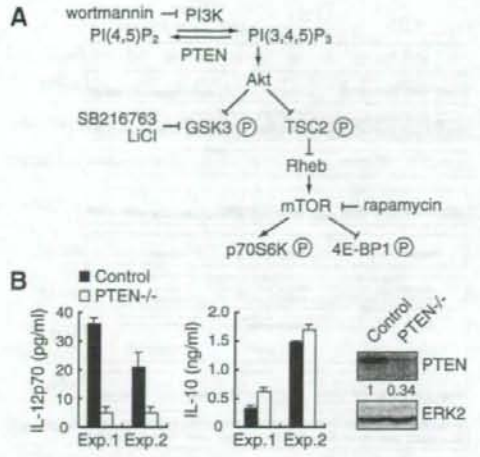

Figure 1. LPS-induced IL-12 production is suppressed in PTEN$^{-/-}$ BMDCs. (A) The overview of PI3K signaling pathway. $PI(4,5)P_2$ indicates phosphatidylinositol(4,5)bisphosphate; $PI(3,4,5)P_3$, phosphatidylinositol-(3,4,5)trisphosphate. (B) BMDCs from PTEN$^{-/-}$ mice (n = 2) or their littermate controls (n = 2) were stimulated with 1 μg/mL LPS for 24 hours and assayed for the production of IL-12p70 and IL-10 by ELISA. Data are indicated as median plus or minus SD. Essentially, the same results were obtained with 2 independent experiments (experiments 1 and 2). The expression levels of PTEN and ERK2 in BMDCs were determined by Western blotting (right panel).

GSK3 pathways in DCs results in the increase and decrease of Th1 responses, respectively.

Methods

Reagents

Lipopolysaccharide (LPS) from *Escherichia coli* 055:B5 was purchased from Sigma-Aldrich (St Louis, MO). Recombinant human (rh) GM-CSF, rhIL-4, rhIL-10, and recombinant mouse (rm) GM-CSF were purchased from PeproTech (Rocky Hill, NJ). Wortmannin, rapamycin, SB216763, cycloheximide, and brefeldin A (BFA) were purchased from Calbiochem (San Diego, CA). Antibodies to ERK2, IκBα, p70S6K, Rheb, GSK3α/β, and STAT3 were purchased from Santa Cruz Biotechnology (Santa Cruz, CA). Antibody to Akt and phosphorylation-specific antibodies to Akt (Ser473), GSK3α/β (Ser21/Ser9), TSC2 (Thr1462), p38 (Thr180/Tyr182), ERK (Thr202/Tyr204), JNK (Thr183/Tyr185), and STAT3 (Tyr705) were purchased from Cell Signaling Technology (Danvers, MA).

Mice

C57BL/6 and BALB/c mice were purchased from Nihon SLC. IL-10$^{-/-}$ mice on a C57BL/6 background were purchased from The Jackson Laboratory (Bar Harbor, ME). Mice deficient for p85α were reported previously.[15,16] Mice had been backcrossed to the BALB/c background for 12 generations. STAT3 mutant (LysM-Cre x STAT3$^{flox/flox}$) mice[17] on a mixed (129 × C57BL/6) background were kindly provided by Dr K. Takeda (Osaka University, Osaka, Japan). STAT3$^{flox/flox}$ or LysM-Cre x STAT3$^{flox/+}$ mice were used as controls. PTEN mutant (LysM-Cre x PTEN$^{flox/flox}$) mice[18,19] on a C57BL/6 background were kindly provided by Dr A. Suzuki (Akita University, Akita, Japan). PTEN$^{flox/flox}$ mice were used as controls. LysM-Cre x STAT3$^{flox/flox}$ and LysM-Cre x PTEN$^{flox/flox}$ mice were referred to here as STAT3$^{-/-}$ and PTEN$^{-/-}$ mice, respectively. Mice were maintained at Taconic Farms (Germantown, NY) or in our animal facility under specific pathogen-free conditions. All experiments were performed in accordance with our institutional guidelines.

Preparation of dendritic cells

To generate bone marrow (BM)–derived DCs (BMDCs), mouse BM cells were cultured at 10^6/mL in complete medium (RPMI 1640; Sigma-Aldrich, 10% fetal calf serum, 55 μM 2-mercaptoethanol, 100 U/mL penicillin, 100 μg/mL streptomycin) supplemented with 10 ng/mL rmGM-CSF for 6 days. The culture medium was changed every 2 days. On day 6, BMDCs were isolated using antimouse CD11c magnetic beads (Miltenyi Biotec, Auburn, CA) with an AutoMACS (Miltenyi Biotec). Human peripheral blood mononuclear cells from normal healthy volunteers were isolated by centrifugation on a Ficoll-Metrizoate density gradient (Lymphoprep; Nycomed, Oslo, Norway). The protocol was approved by the local ethics committee at Keio University School of Medicine, and informed consent was obtained from donors in accordance with the Declaration of Helsinki. Monocytes were then isolated using antihuman CD14 magnetic beads (Miltenyi Biotec) with an AutoMACS, followed by incubation at 10^6 cells/mL in complete medium supplemented with 100 ng/mL rhGM-CSF and 100 ng/mL rhIL-4 for 6 days, to obtain monocyte-derived DCs (MDDCs).

Western blotting

Western blotting was carried out as described.[8] To detect phospho-STAT3 and phospho-TSC2, immunoreaction enhancer (Can Get Signal, Toyobo, Japan) was added to the reaction according to the manufacturer's instructions. ERK2 was used as a loading control. A LAS-3000 imaging system (Fuji) was used to produce digital images. Signal intensities (for phospho-STAT3) and signal profiles (for p70S6K) were quantified with Image Gauge software version 4.1 (Fuji).

Enzyme-linked immunosorbent assay

Cytokine concentrations in the culture supernatants were quantified by enzyme-linked immunosorbent assay (ELISA; Quantikine; R&D Systems, Minneapolis, MN).

Quantitative real-time polymerase chain reaction

Total RNA was prepared using NucleoSpin RNA II (Macherey-Nagel, Düreu, Germany), and cDNA was synthesized with Ready-To-Go T-Primed First-Strand kit (GE Healthcare, Chalfont St Giles, United Kingdom). Quantitative real-time polymerase chain reaction (PCR) was performed by applying the real-time SYBR Green PCR technology using SYBR premix Ex Taq (Takara, Otsu, Japan) with specific primers on an iCycler IQ (Bio-Rad, Hercules, CA). PCR cycling was as follows: 95°C for 10 seconds for 1 cycle, 95°C for 5 seconds, 58°C for 20 seconds, 72°C for 15 seconds for 40 cycles, and 70°C for 5 minutes. Amplification of cyclophilin A mRNA was done for each sample as an endogenous control. Primer pairs specific for IL-12p40 (forward, CAGAAGCTAACCATCTCCTGGTTTG; reverse, CCGGAGTAATTTGGTGCTCCACAC), IL-12p35 (forward, TCACATCTCATCTCCCCAAA; reverse, TCTGCTAACACATTGAGGGG), IL-10 (forward, GGTTGCC-AAGCCTTATCGGA; reverse, ACCTGCTCCACTGCCTTGCT), interferon-β (IFN-β) (forward, CCATCCAAGAGATGCTCCAG; reverse, GTGGAGAGCAGTTGAGGACA), suppressor of cytokine signaling 3 (SOCS3) (forward, GGGGGAGGCAGGAGGTGATGGA; reverse, GGGCGGGCTGGAGGTGGATT) and cyclophilin A (forward, ATGGCACTGGCGGCAGGTCC; reverse, TTGCCATTCCTGGACCCAAA) were used.

Preparation of lentiviral vectors

The following constructs were kindly provided by Dr H. Miyoshi (RIKEN, Tsukuba, Japan): CSII-EF-MCS-IRES2-Venus, a self-inactivating lentiviral construct; pCAG-HIVgp and pCMV-VSVG-RSV-Rev, packaging constructs.[20] This lentiviral system is designed to express a desired gene under the direction of the elongation factor-1 promoter along with internal ribosomal entry site (IRES)-driven Venus, a derivative of YFP,[21] as a marker for monitoring the infection efficiency. Mouse Rheb was amplified by PCR using cDNA from the brain of C57BL/6 mice as a template (5′

primer, ATGCCTCAGTCCAAGTCCCG; 3′ primer, TCACATCACCGAGCACGAAG) and cloned into the pGEM-T Easy vector (Promega, Madison, WI). After sequence verification, the construct was subjected to PCR mutagenesis to obtain Rheb Q64L, a constitutively active form of Rheb, Glu-64 replaced by Leu. The product was verified by DNA sequencing and subcloned into CSII-EF-MCS-IRES2-Venus. For the generation of lentiviral vectors, 293T cells were transfected with CSII-EF-MCS-IRES2-Venus with or without Rheb Q64L insert, pCAG-HIVgp, and pCMV-VSUG-RSV-Rev using Lipofectamine 2000 (Invitrogen, Carlsbad, CA). After 2 days, culture supernatants were passed through a 0.45-μm filter, condensed to 0.5% volume, and used for gene transduction.

Generation of gene-transduced BMDCs

Mouse BM cells were incubated with phycoerythrin-conjugated antibodies against CD3ε, CD4, CD8α, CD11b, Gr-1, B220, and TER119 (BD Biosciences, San Jose, CA) along with anti-phycoerythrin microbeads (Miltenyi Biotec), followed by negative selection with an AutoMACS. The remaining cells (0.5×10^5 cells/0.5 mL) were cultured with 10 ng/mL rmGM-CSF in a 24-well plate for 2 days, followed by spin infection (1800 rpm, 2 hours) with 40 μL of each viral vector along with 5 μg/mL polybrene. After infection, each well was split into 2 wells (2 mL/well) and cultured with 10 ng/mL rmGM-CSF for another 4 days. The culture medium was changed every 2 days. The cells were then harvested, washed, and incubated with allophycocyanin-conjugated antimouse CD11c monoclonal antibody (mAb), and Venus-as well as CD11c-positive cells were sorted as gene-transduced BMDCs using a FACSAria (BD Biosciences). The purity was estimated to be more than 85%.

CD4+ T-cell priming

Human MDDCs (1×10^6 cells) were incubated in the presence or absence of 10 μg/mL tuberculin purified protein derivative (PPD) for 1 hour, and subsequently stimulated with or without 1 μg/mL of LPS along with or without 100 nM of rapamycin. After 2 hours of stimulation, the cells were harvested, washed, and cultured (3×10^5 cells) for a week with CD4+ T cells from the same donor (3×10^6 cells), which were isolated from peripheral blood mononuclear cells using antihuman CD4 magnetic beads (Miltenyi Biotec) with an AutoMACS. CD4+ T cells were then restimulated with antihuman CD3ε (10 μg/mL) and antihuman CD28 (1 μg/mL) mAbs for 48 hours.

Leishmania major infection

L major infection was performed as described.[8,22] Two days after infection, 40 μL of 2 mM LiCl/phosphate-buffered saline (PBS) or PBS were injected into the infected left hind footpad subcutaneously.

Results

Products of PI3K are involved in the regulation of IL-12 expression

To prove that the lipid kinase activity of PI3K regulates IL-12 production, we examined the role of PTEN, which catalyzes a reaction opposite to PI3K (Figure 1A). BMDCs lacking PTEN produced lower amounts of IL-12 than control BMDCs on LPS stimulation (Figure 1B), indicating that the products of PI3Ks, phosphatidylinositol(3,4,5)trisphosphate in particular, are indeed critical for the regulation of IL-12 expression.

Activation of mTOR and GSK3 pathways by LPS stimulation of DCs

We examined the signaling components of PI3K-Akt pathway in LPS-stimulated BMDCs (Figure 1A). As shown in Figure 2, LPS stimulation induced the phosphorylation of TSC2 and GSK3, known targets of Akt. The activation of mTOR was evaluated by the phosphorylation of p70S6K. Consistent with the fact that mTOR is activated by serum and nutrients, p70S6K was partially phosphorylated even without LPS (Figure 2 lane 1). The hyperphosphorylation of p70S6K examined by electrophoretic mobility shifts was induced within 10 minutes (Figure 2 lane 2) and became clearer up to 60 minutes after LPS stimulation (Figure 2 and Figure S1 lane 4, available on the *Blood* website; see the Supplemental Materials link at the top of the online article; note that the electrophoretic mobility of p70S6K shifts from a and b up to c and d bands). Rapamycin completely blocked the phosphorylation of p70S6K (Figures 2, S1, compare lanes 1-4 and 9-12). In contrast, rapamycin had no effect on the LPS-induced phosphorylation of Akt and TSC2 (Figure 2 lanes 9-12), which is consistent with the fact that Akt and TSC2 act upstream of mTOR (Figure 1A). Wortmannin, an inhibitor of PI3K, only partially blocked the LPS-induced phosphorylation of p70S6K (Figures 2, S1, lanes 5-8), whereas the phosphorylation of Akt and TSC2 was completely inhibited (Figure 2 lanes 5-8). These data suggest that LPS-induced mTOR activation is mediated by both PI3K-dependent and-independent pathways, the latter of which could involve serum and/or nutrients.

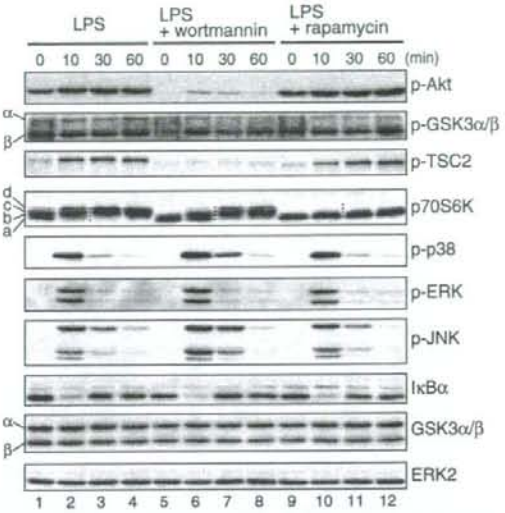

Figure 2. The PI3K signaling pathway is activated by LPS in BMDCs. BMDCs were cultured overnight and then pretreated with either 100 nM wortmannin or 10 ng/mL rapamycin for 20 minutes or left untreated before being stimulated with 1 μg/mL LPS for the indicated times. Cell lysates were analyzed for phospho-Akt, phospho-GSK3α/β, phospho-TSC2, p70S6K, phospho-p38, phospho-ERK, phospho-JNK, IκBα, GSK3α/β, and ERK2 by Western blotting. Four dots added between the 10-minute and 30-minute lanes of p70S6K samples indicate the migration positions of hyperphosphorylated p70S6K caused by multiple phosphorylation events, which are represented as a through d on the left side (Figure S1).

GSK3 activity is negatively regulated by Akt-mediated phosphorylation.[23] We found that GSK3β was predominantly phosphorylated on LPS stimulation in BMDCs, whereas both GSK3α and GSK3β were expressed (Figure 2 lanes 1-4). The effect of wortmannin on GSK3β phosphorylation was partial (Figure 2 lanes 5-8), indicating that the LPS-induced phosphorylation of GSK3β was also mediated by both PI3K-dependent and -independent pathways. As expected, rapamycin had no effect on the LPS-induced phosphorylation of GSK3β (Figure 2 lanes 9-12).

We also examined the effects of rapamycin and wortmannin on LPS-activated MAPK and NF-κB pathways. Rapamycin had little effect on the phosphorylation status of MAPK family members or the degradation of IκBα, a measure of NF-κB activation (Figure 2, compare lanes 1-4 and lanes 9-12). In contrast, consistent with previous reports,[8,24,25] wortmannin slightly but reproducibly enhanced the LPS-induced phosphorylation of p38 as well as JNK (Figure 2, compare lanes 3 and 7), indicating that a PI3K-dependent but mTOR-independent pathway(s) negatively regulates the activation of p38 and JNK. Wortmannin had little effect on IκBα degradation, indicating that the NF-κB pathway is probably not the target of PI3K pathway in BMDCs.

Rapamycin augments LPS-induced IL-12 production but suppresses IL-10 production in an mTOR-dependent manner

We next examined the role of mTOR in the regulation of IL-12 expression. As shown in Figure 3A, the treatment of BMDCs with rapamycin as well as wortmannin enhanced LPS-induced IL-12p70 production. In contrast, LPS-induced IL-10 production was suppressed by rapamycin or wortmannin, and the effect of rapamycin was more potent than wortmannin (Figure 3A). Rapamycin had the same effect on human MDDCs (Figure S2). On the other hand, rapamycin and wortmannin had little effect on the production of IL-6 and tumor necrosis factor-α (TNF-α; Figure 3A). PTEN$^{-/-}$ BMDCs produced slightly more IL-10 compared with control BMDCs (Figure 1B), but the effect of PTEN deficiency is more pronounced on IL-12 compared with IL-10 production.

A complex of rapamycin and FK506-binding protein 12 (FKBP12) binds to and inhibits mTOR. Because FK506 competes with rapamycin for binding to FKBP12, the excess amounts of FK506 cancel the biologic actions of the rapamycin-FKBP12 complex.[26] Indeed, FK506 prevented the rapamycin-induced augmentation of IL-12p70 and IL-12p40 production in a dose-dependent manner (Figure 3B). The suppression of IL-10 production by rapamycin was also canceled with excess FK506 (Figures 3B, S3). Excess amounts of FK506 partially restored the hyperphosphorylation of p70S6K (Figure S3). These results confirm that the effect of rapamycin on cytokine production is mediated by the inhibition of mTOR function.

We further examined the effects of wortmannin and rapamycin on LPS-induced cytokine mRNA expression, including IL-12p40, IL-12p35, IL-10, and IFN-β by real-time RT-PCR (Figure 3C). Consistent with these results, the expression of both IL-12p40 and IL-12p35 mRNAs was enhanced by wortmannin and rapamycin. In contrast, IL-10 mRNA expression was suppressed only by rapamycin. Interestingly, wortmannin but not rapamycin enhanced LPS-induced IFN-β mRNA expression. These results collectively suggest that the PI3K regulates the expression of distinct sets of cytokine genes expression in mTOR-dependent and -independent pathways.

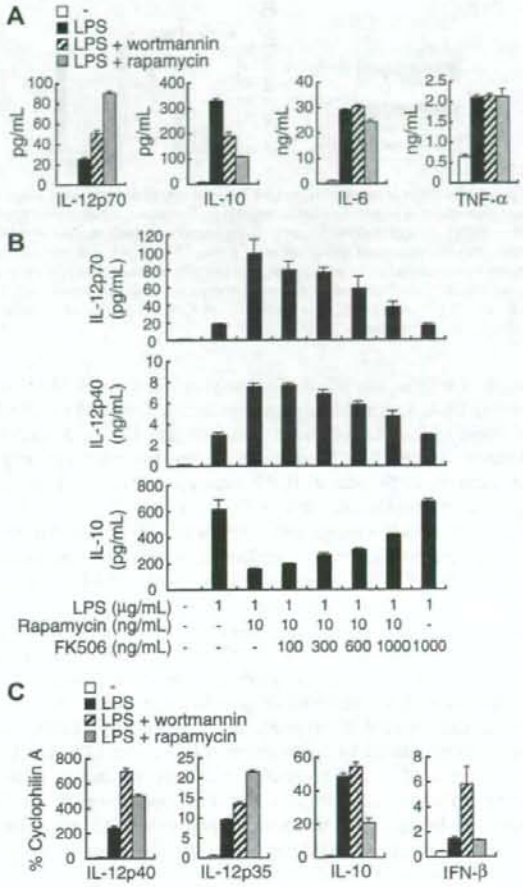

Figure 3. The effect of rapamycin on LPS-induced cytokine expression in BMDCs. (A) BMDCs were stimulated with 1 μg/mL LPS in the presence or absence of either 100 nM wortmannin or 10 ng/mL rapamycin for 24 hours and assayed for the production of IL-12p70, IL-10, IL-6, and TNF-α by ELISA. (B) BMDCs were stimulated with 1 μg/mL LPS with or without 10 ng/mL rapamycin along with the indicated concentrations of FK506 for 24 hours and assayed for the production of IL-12p70, IL-12p40, and IL-10 by ELISA. (C) BMDCs were pretreated with or without either 100 nM wortmannin or 10 ng/mL rapamycin for 20 minutes before stimulation with 1 μg/mL LPS. After 4 hours, total RNA was isolated, and IL-12p40, IL-12p35, IL-10, and IFN-β mRNA levels were assessed by real-time PCR using cyclophilin A mRNA as a reference. All data are indicated as median plus or minus SD of duplicate samples. Similar results were obtained with 2 to 4 independent experiments.

Constitutively active Rheb affects the regulation of cytokine production

To further confirm the role of mTOR in cytokine gene regulation, we used a lentiviral vector-mediated gene delivery system[20] to activate mTOR by expressing a constitutively active form of Rheb (Rheb Q64L).[27] The phosphorylation-induced electrophoretic mobility shift of p70S6K in untreated and LPS-stimulated DCs was augmented in BMDCs expressing Rheb Q64L compared with control BMDCs (Figure 4A and Figure S4 lanes 1 and 3, lanes 2 and 4), confirming the activity of Rheb Q64L. As shown in Figure 4B, LPS-induced IL-12p70 production was decreased in Rheb Q64L-expressing BMDCs compared with mock-infected BMDCs. In contrast, LPS-induced IL-10 production was increased in Rheb Q64L-expressing BMDCs. No difference in IL-6 production was observed (data not shown). These results indicate that mTOR is indeed involved in the regulation of IL-12 and IL-10 production in LPS-stimulated BMDCs.

The effect of rapamycin on IL-12 expression involves IL-10 in an autocrine manner

Because mTOR is involved in diverse biologic processes, including protein synthesis and gene expression,[14] it is possible that mTOR regulates IL-12 gene expression through new protein synthesis. When BMDCs were treated with cycloheximide to inhibit de novo

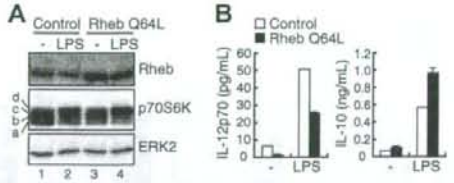

Figure 4. The effect of Rheb Q64L on LPS-induced cytokine production. BMDCs were infected with a lentivirus vector expressing a constitutively active form of Rheb (Rheb Q64L) or vector alone (control). Gene-transduced BMDCs were isolated ("Methods") and stimulated with or without 1 μg/mL LPS for 24 hours. (A) The cell lysates were analyzed for Rheb, p70S6K, and ERK2 by Western blotting. Note that the mobility shifts of p70S6K caused by multiple phosphorylation are represented as a through d (Figure S4). (B) The production of IL-12p70 and IL-10 in culture supernatants was assayed by ELISA.

protein synthesis, the effect of rapamycin was reduced (data not shown). BFA, which blocks protein secretion, abrogated the effect of rapamycin on LPS-induced IL-12p40 and IL-12p35 mRNA expression (Figure 5A). These results strongly suggest that rapamycin controls LPS-induced IL-12 expression through a newly synthesized autocrine mediator(s).

IL-10 is an anti-inflammatory cytokine capable of inhibiting the LPS-induced production of proinflammatory cytokines, including IL-12 in DCs.[28] When we examined the kinetics of LPS-induced IL-12 and IL-10 expression, rapamycin augmented IL-12p40 and IL-12p35 mRNA expression at 4 hours but not 2 hours after LPS stimulation (Figure 5B). On the other hand, the rapamycin-induced suppression of IL-10 mRNA expression was already observed at 2 hours after LPS stimulation (Figure 5B). Consistent with these results, LPS-induced IL-10 production evaluated by ELISA was significantly reduced by rapamycin at 4 hours after LPS stimulation, whereas IL-12p40 production was little affected (data not shown). These results suggest that the suppression of IL-10 expression by rapamycin subsequently augments IL-12 expression.

To test this hypothesis further, we examined whether rapamycin attenuates the IL-10 signaling pathway in LPS-stimulated DCs. For this purpose, we analyzed the phosphorylation status of STAT3 at Tyr705 as a measure of IL-10 signaling. We found that the tyrosine phosphorylation of STAT3 was markedly induced at 2 hours after LPS stimulation, which was inhibited by rapamycin (Figure 5C). Similar results were obtained in human MDDCs (Figure S5). To rule out the possibility that rapamycin directly inhibits the STAT3 signaling pathway, we examined the effect of rapamycin on the IL-10–induced expression of SOCS3, a well-known target of the STAT3 signaling pathway.[29] As shown in Figure 5D, SOCS3 mRNA expression induced by IL-10 stimulation was unaffected by rapamycin. Collectively, these results indicate that rapamycin directly suppresses LPS-induced IL-10 expression but not the STAT3 signaling pathway.

To confirm that rapamycin works through the IL-10-STAT3 pathway to down-regulate IL-12 expression, we used IL-$10^{-/-}$ and STAT$3^{-/-}$ DCs. As shown in Figure 5E, the effect of rapamycin was virtually absent in IL-$10^{-/-}$ BMDCs (1.2 ± 0.03-fold increase) compared with WT BMDCs (3.8 ± 0.1-fold increase). Essentially the same result was obtained with STAT$3^{-/-}$ BMDCs (Figure 5F, 3.3 ± 0.2-fold increase in control BMDCs vs 1.2 ± 0.1-fold increase in STAT$3^{-/-}$ BMDCs). The production of IL-12p70 from IL-$10^{-/-}$ DCs was strongly suppressed by the addition of exogenous IL-10, and such inhibition was rapamycin-independent (Figure S6). These results clearly indicate that rapamycin enhances IL-12 production through the inhibition of autocrine IL-10 action in LPS-stimulated BMDCs.

mTOR and GSK3 cooperatively regulate LPS-induced IL-12 production

As wortmannin had only a marginal effect on LPS-induced phosphorylation of p70S6K (Figure 2) as well as IL-10 expression (Figure 3A,C), we examined pathways other than mTOR that lie downstream of PI3K. Indeed, GSK3 has been reported to regulate the TLR-mediated production of cytokines, such as IL-12p40 and IL-10 in human monocytes and DCs.[30,31] We therefore examined whether GSK3 regulates LPS-induced cytokine production in mouse BMDCs using SB216763, a specific GSK3 inhibitor. SB216763 attenuated IL-12p70 production but enhanced IL-10 production by LPS-stimulated DCs (Figure 6A, lane 5). We obtained similar results with another GSK3 inhibitor LiCl (data not shown). These data indicate that PI3K regulates IL-12 production through both mTOR and GSK3 pathways and that GSK3 positively regulates LPS-induced IL-12p70 and negatively regulates IL-10 production in BMDCs.

Given that the PI3K-Akt pathway negatively regulates GSK3 (Figure 1A), the treatment of cells with wortmannin should activate GSK3. Interestingly, wortmannin augmented the effect of rapamycin on LPS-induced IL-12p70 production (Figure 6A lanes 2-4 and 6). On the other hand, consistent with the marginal effect of wortmannin alone (Figure 6A lane 3), wortmannin failed to augment the suppressive effect of rapamycin on LPS-induced IL-10 production (Figure 6A lanes 2-4 and 6), suggesting that mTOR and GSK3 differentially regulate IL-12 production. Wortmannin had little effect on LPS-induced IL-12p70 and IL-10 production in the presence of SB216763 (Figure 6A lanes 5 and 7). It is probable that the contribution of GSK3 is similar to or greater than that of mTOR for the regulation of IL-12 production in DCs. Consistent with those observations, LPS-induced IL-12p70 production was decreased in the presence of SB216763 in IL-$10^{-/-}$ BMDCs (Figure 6B). These results collectively indicate that GSK3 directly regulates LPS-induced IL-12 production independent of IL-10 (Figure 6C).

Attenuation of mTOR and GSK3 affects Th1/Th2 balance

Because IL-12 is critical for triggering Th1 responses, our results raise an interesting possibility that blocking mTOR and GSK3 may enhance and diminish Th1 responses, respectively. Human peripheral $CD4^+$ T cells stimulated with MDDCs pretreated with LPS plus PPD in the presence of rapamycin produced more IFN-γ on restimulation with anti-CD3 plus anti-CD28 antibodies than $CD4^+$ T cells stimulated with DCs pretreated in the absence of rapamycin (Figure 7A). It is thus probable that treatment of DCs with rapamycin results in the augmentation of a Th1 response presumably through enhanced IL-12 production and reduced IL-10 production. We next examined the effect of GSK3 inhibition in an in vivo infection model with *L major*, in which adequate Th1 development is required for disease control.[22] We have previously shown that Th2 prone BALB/c mice can elicit a reasonable Th1 response on *L major* infection in the absence of p85α (Fukao et al[8] and Figure 7B, compare open triangles and open circles). Because GSK3 is expected to have an increased activity in the absence of p85α, we administered a GSK3 inhibitor, LiCl, into footpad of p85$\alpha^{-/-}$ mice on a BALB/c background when infected with *L major*. As shown in Figure 7B, whereas p85$\alpha^{-/-}$ BALB/c mice were resistant to infection, the administration of LiCl to p85$\alpha^{-/-}$ BALB/c mice resulted in increased footpad swelling and animals were no longer able to control the infection. These results

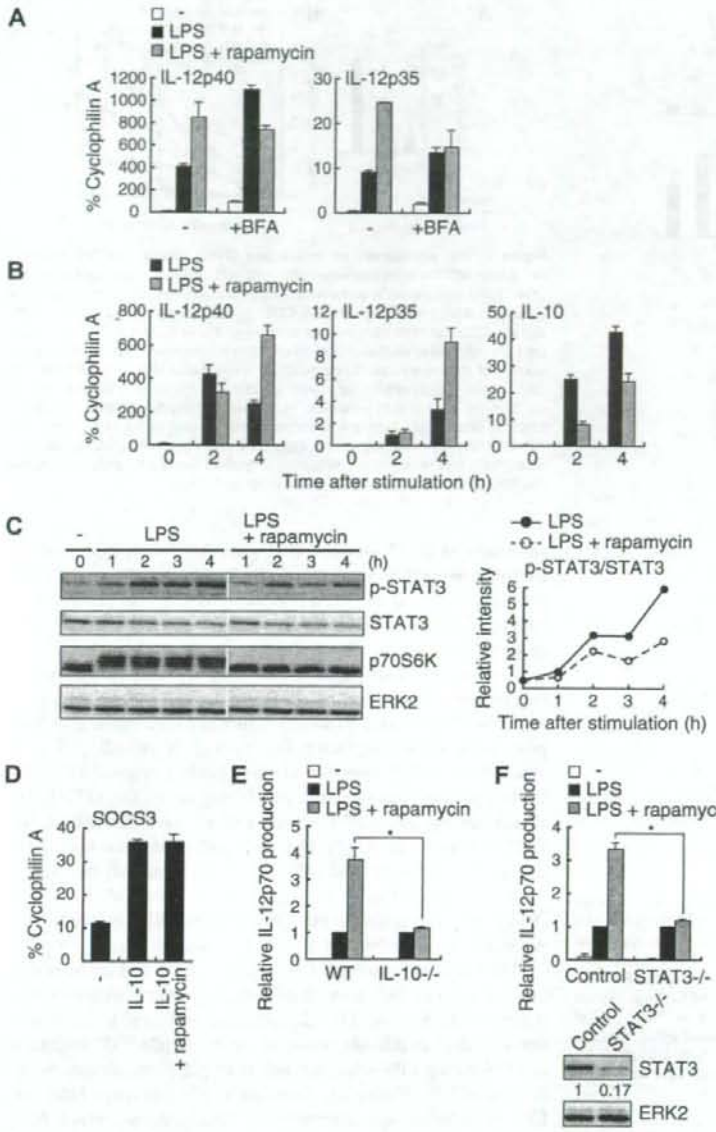

Figure 5. The effect of rapamycin on LPS-induced IL-12 production depends on the IL-10–STAT3 signaling pathway. (A) BMDCs were pretreated with or without 10 ng/mL rapamycin along with or without 5 μg/mL BFA for 20 minutes before stimulation with 1 μg/mL LPS. After 4 hours, total RNA was isolated, and IL-12p40 and IL-12p35 mRNA levels were assessed by real-time PCR using cyclophilin A mRNA as a reference. (B) BMDCs were pretreated with or without 10 ng/mL rapamycin for 20 minutes and then stimulated with 1 μg/mL LPS for the indicated times. Total RNA was isolated, and IL-12p40, IL-12p35, and IL-10 mRNA levels were assessed by real-time PCR using cyclophilin A mRNA as a reference. (C) BMDCs were pretreated with or without 100 ng/mL rapamycin for 20 minutes and then stimulated with 1 μg/mL LPS for the indicated times. The cell lysates were analyzed for phospho-STAT3, STAT3, p70S6K, and ERK2 by Western blotting. The white lines indicate that intervening lanes have been removed. The right panel indicates relative intensities of tyrosine-phosphorylated STAT3 normalized by STAT3 signals. (D) BMDCs were pretreated with or without 100 ng/mL rapamycin for 20 minutes before stimulation with 10 ng/mL IL-10. After 1 hour, total RNA was isolated, and SOCS3 mRNA levels were assessed by real-time PCR using cyclophilin A mRNA as a reference. In panels A, B, and D, data are indicated as mean plus or minus SD of duplicate samples. Data are representative of 2 (B,C) or 3 (A,D) independent experiments with similar results. (E) BMDCs from WT or IL-10$^{-/-}$ mice were stimulated with 1 μg/mL LPS in the presence or absence of 10 ng/mL rapamycin for 24 hours and assayed for the production of IL-12p70 by ELISA. Absolute IL-12p70 levels in the stimulation of LPS alone: WT, 24.1 plus or minus 3.6 pg/mL; IL-10$^{-/-}$, 1120 plus or minus 230 pg/mL. Data are indicated as median plus or minus SD of 3 independent experiments. *$P < .05$ by Mann-Whitney U test comparing WT with IL-10$^{-/-}$ groups. (F) BMDCs from STAT3$^{-/-}$ mice or littermate controls were stimulated with 0.1 μg/mL LPS in the presence or absence of 100 ng/mL rapamycin for 24 hours. Cytokine production was evaluated as in panel E. Absolute IL-12p70 levels in the stimulation of LPS alone: control, 11.8 plus or minus 3.7 pg/mL; STAT3$^{-/-}$, 299 plus or minus 67 pg/mL. *$P < .05$ by Mann-Whitney U test comparing control with STAT3$^{-/-}$ groups. Indicated below are the expression levels of STAT3 and ERK2 in BMDCs determined by Western blotting.

collectively indicate that the attenuation of mTOR and GSK3 by inhibitors affects the balance between Th1 and Th2 responses.

Discussion

We have previously shown that PI3K negatively regulates TLR-induced pro-inflammatory cytokine production by DCs and gut epithelial cells.[8,9,25] Because LPS-induced IL-12 production was decreased in PTEN$^{-/-}$ BMDCs (Figure 1B), the PI3K-Akt pathway triggered by the lipid product of PI3K is indeed important for the suppression of LPS-induced IL-12 production.

Furthermore, our results show that the PI3K-Akt pathway positively regulates IL-10 production. IL-10 is produced by various cell types and plays anti-inflammatory roles in many immune responses.[32] In particular, it has been shown that DC-derived IL-10 is involved in a variety of responses, such as infectious diseases,[33] the induction of tolerance,[34] and cytotoxic T-lymphocyte–mediated antitumor activity.[32] Considering that IL-10 plays a pivotal role in immune regulation, the elucidation of the molecular mechanism underlying PI3K-mediated IL-10 regulation would shed new light on therapeutic approaches toward cancer as well as autoimmune diseases.

Indeed, signaling molecules involved in the PI3K pathway (ie, mTOR and GSK3) seem reasonable targets for appropriately modulating the Th1/Th2 balance. As shown here, the treatment of DCs with rapamycin augments a Th1 response (Figure 7A). Because rapamycin does not alter antigen uptake

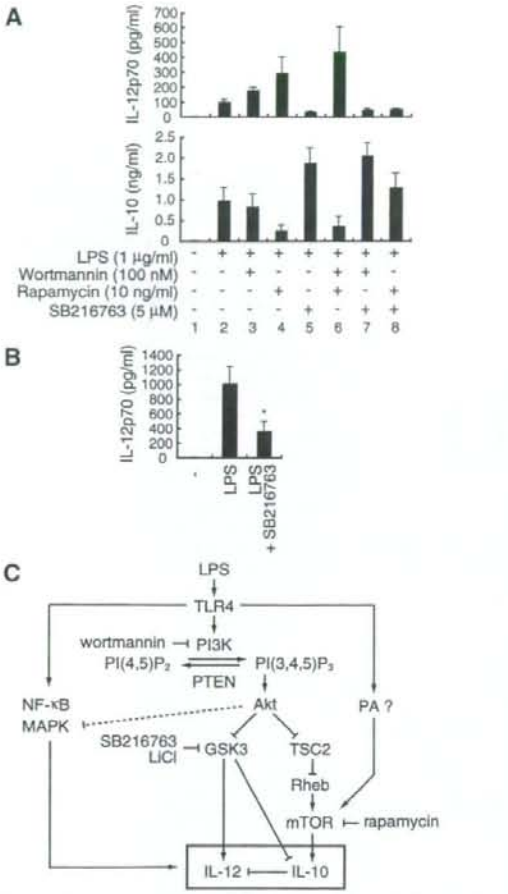

Figure 6. mTOR and GSK3β regulate LPS-induced IL-12 production through distinct mechanisms. (A) BMDCs were stimulated with 1 μg/mL LPS together with the indicated inhibitors for 24 hours and assayed for the production of IL-12p70 and IL-10 by ELISA. Data are indicated as median plus or minus SD of 3 independent experiments. (B) BMDCs from IL-10$^{-/-}$ mice were stimulated with 1 μg/mL LPS in the presence or absence of 5 μM SB216763 for 24 hours and assayed for the production of IL-12p70 by ELISA. Data are indicated as median plus or minus SD of 5 independent experiments. *$P < .05$ by Wilcoxon t test compared with LPS alone. (C) The schematic diagram of the PI3K-mediated regulation of IL-12 production. PA indicates phosphatidic acid; $PI(4,5)P_2$, phosphatidylinositol(4,5)bisphosphate; $PI(3,4,5)P_3$, phosphatidylinositol(3,4,5)trisphosphate.

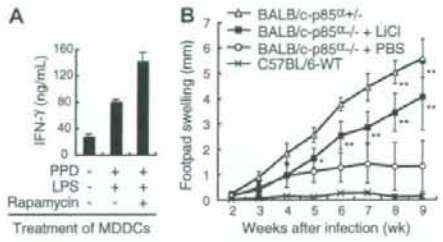

Figure 7. The attenuation of mTOR and GSK3 affects Th1/Th2 balance. (A) Human MDDCs were pretreated with PPD and LPS with or without rapamycin. CD4$^+$ T cells from the same donor were cultured with those MDDCs in the absence of rapamycin. After 1 week of incubation, CD4$^+$ T cells were stimulated with anti-CD3ε and anti-CD28 mAbs for 48 hours and assayed for the production of IFN-γ by ELISA. Data are indicated as median plus or minus SD of duplicate samples. (B) The footpad swelling of *L major*–infected BALB/c-p85α$^{-/-}$ mice treated with LiCl ($n = 8$) or with PBS ($n = 6$) was monitored on a weekly basis. BALB/c-p85α$^{+/-}$ mice ($n = 5$) or C57BL/6-WT mice ($n = 2$) were used as positive and negative controls for *L major* infection, respectively. Data are indicated as median plus or minus SD. *$P < .05$, **$P < .01$ by Mann-Whitney U test compared with PBS-treated BALB/c-p85α$^{-/-}$ mice. There was no significant difference in footpad swelling between LiCl-treated BALB/c-p85α$^{-/-}$ mice and untreated BALB/c-p85α$^{+/-}$ mice.

and presentation,[35] or the expression level of costimulatory molecules such as CD80 and CD86 in DCs,[36] the enhancement of a Th1 response by rapamycin is probably the result of the augmentation of IL-12 production. In addition, the inhibition of GSK3 by LiCl suppressed a Th1-mediated immune response against *L major* in vivo (Figure 7B). These results raise the possibility that the attenuation of these signaling pathways may provide new therapeutic approaches for human diseases.

Based on our present studies as well as other reports, we propose that signal transduction pathways downstream of Akt regulating IL-12 production are composed of at least 3 components: mTOR, GSK3, and MAPK (Figure 6C). First, the mTOR pathway negatively regulates IL-12 production through the induction of IL-10 gene expression. Wortmannin did not completely inhibit the LPS-induced phosphorylation of p70S6K (Figure 2), and a combination of wortmannin and rapamycin further enhanced LPS-induced IL-12 production (Figure 6A), suggesting that the LPS-induced mTOR activation depends only partially on the PI3K pathway. It should be noted that phosphatidic acid produced by LPS stimulation in macrophages activates mTOR in a PI3K-independent manner[37] (Figure 6C).

Second, the GSK3 pathway positively regulates IL-12 production in a more direct manner. Using human monocytes, Martin et al[30] showed that GSK3 positively regulates LPS-induced IL-12p40 production. GSK3 augments the binding of NF-κB p65 to a coactivator "cAMP response element-binding protein" (CREB)-binding protein by competitively inhibiting the binding of CREB to CREB-binding protein.[30] Rodionova et al[31] have also shown that GSK3 enhances IL-12p70 and IL-12p40 production by human *Escherichia coli*–activated MDDCs. Considering that the GSK3-mediated regulation of IL-12 production was independent of IL-10 (Figure 6B), it is probable that GSK3 controls LPS-induced IL-12 production by a mechanism distinct from mTOR.

Third and finally, we and others have reported that the treatment of monocytes or DCs with SB203580, a specific inhibitor of p38, suppressed LPS-induced IL-12 production.[8,11,38] In addition, consistent with the fact that Akt negatively regulates p38,[39] the inhibition of PI3K during LPS activation enhanced p38 phosphorylation and activation[8,24,25] (Figure 2). Conversely, p38 phosphorylation on LPS stimulation was decreased in macrophages derived from PTEN$^{-/-}$ mice.[40] These observations suggest that the PI3K-mediated suppression of p38 results in the attenuation of IL-12 production as well. It has also been reported that the PI3K-Akt pathway negatively regulates JNK activity.[41] Indeed, the treatment of BMDCs with wortmannin slightly enhanced LPS-induced JNK phosphorylation (Figure 2). Studies regarding the function of JNK in LPS-induced IL-12 production using human monocyte cell lines are controversial,[42,43] and the role of JNK in LPS-induced IL-12 production should be evaluated in primary cells, such as BMDCs derived from JNK-deficient mice. Given that rapamycin (Figure 2) and SB216763 (data not shown) had no effect on LPS-induced phosphorylation of p38 and JNK, it seems improbable that mTOR or GSK3 is involved in the PI3K-Akt pathway-mediated negative regulation of p38 and JNK activity. These results taken together indicate that mTOR, GSK3, and MAPK cooperatively regulate TLR-induced IL-12 production in DCs (Figure 6C).

In contrast to IL-10, IFN-β enhances IL-12 production in an autocrine manner.[44] Because wortmannin augments the expression of IFN-β in response to LPS (Figure 3C), it is possible that wortmannin enhances IL-12 production through IFN-β. However, whereas wortmannin enhances the expression of both IL-12p40 and IL-12p35, IFN-β enhances the expression of IL-12p35 but not IL-12p40,[44] suggesting that the effect of wortmannin is probably not mediated by IFN-β. In contrast to wortmannin, rapamycin affected only IL-10 but not IFN-β gene expression (Figure 3C).

Because IL-10 inhibits the LPS-induced production of a diverse array of cytokines, such as IL-6 and TNF-α in addition to IL-12,[28] rapamycin may influence the production of these cytokines. However, we found that rapamycin had no effect on LPS-induced IL-6 and TNF-α production (Figure 3A), consistent with a previous observation that the LPS-induced mRNA expression of IL-12p40, but not TNF-α, is decreased in BMDCs expressing a constitutively active STAT3.[45] Although not shown, rapamycin also augmented IL-12p40 production and suppressed IL-10 production in mouse BMDCs in response to other TLR ligands, such as zymosan (for TLR2/6) and CpG-ODN (for TLR9), whereas it had no effect on IL-6 production. It is possible that the expression of those cytokines has different sensitivities to the negative regulation by IL-10.

What is the molecular mechanism underlying the PI3K-mediated regulation of LPS-induced IL-10 production? p70S6K, one of the targets regulated by mTOR, is able to increase the translation of a subset of mRNAs that contain a 5′ tract of oligopyrimidine.[46] However, the 5′ tract of oligopyrimidine was not detected in mouse or human IL-10 mRNA. Another target molecule, 4E-BP1, regulates eIF-4E, which stimulates translational initiation but whose function is thought to be general and not restricted to a subset of genes. mTOR is also involved in gene transcription through the regulation of transcriptional factors without a translational event.[14,47,48] This mechanism is more probable because our observations indicate that rapamycin suppresses LPS-induced IL-10 production at a transcriptional level (Figure 3C), rather than through translational regulators. However, the DNA binding of transcriptional factor Sp1 to the *IL10* promoter in LPS-stimulated mice BMDCs was unaffected in the presence of rapamycin (data not shown). The regulation by transcription factors downstream of mTOR remains to be elucidated in future studies. In addition to mTOR, GSK3 is involved in a regulatory pathway for IL-10 production. Indeed, GSK3 negatively regulated LPS-induced IL-10 production (Figure 6A), presumably by inactivation of CREB,[30] which is involved in the transcriptional activation of the *IL10* gene.

It should be noted that many previous studies on the regulation of IL-10 or IL-12 gene expression were performed using macrophage or DC cell lines. We have been aware that cell lines and primary cells often showed different results. One obvious problem is the fact that many cell lines have some defect or alteration in PI3K-PTEN regulation, such that many immortalized cell lines lack PTEN expression and show enhanced Akt activity. These cells are obviously not suitable for studying PI3K pathways. Detailed analysis with primary cells is important in future studies.

Acknowledgments

The authors thank Drs A. Suzuki, H. Miyoshi, and K. Takeda for valuable materials, Dr T. Luft of German Cancer Research Center for valuable discussion and sharing unpublished data, and Dr Linda K. Clayton of Harvard Medical School for critically reading the manuscript.

This work was supported by the Uehara Memorial Foundation, a Keio Gijuku Academic Development Fund (S. Matsuda), a Grant-in-Aid for Scientific Research (C 19590499; S. Matsuda) from the Japan Society for the Promotion of Science, a Grant-in-Aid for Scientific Research on Priority Areas (14021110 and 18073015), a National Grant-in-Aid for the Establishment of a High-Tech Research Center in a private university, and a Scientific Frontier Research Grant from the Ministry of Education, Culture, Sports, Science and Technology, Japan.

Authorship

Contribution: M.O. designed the research, performed experiments, and wrote the paper; S.N., S. Kondo, S. Mizuno, K.N., and M.T. performed experiments; T.T. and S. Matsuda designed the research; and S. Koyasu designed the research and wrote the paper.

Conflict-of-interest disclosure: The authors declare no competing financial interests.

Correspondence: Shigeo Koyasu, Department of Microbiology and Immunology, Keio University School of Medicine, 35 Shinanomachi, Shinjuku-ku, Tokyo 160-8582, Japan; e-mail: koyasu@sc.itc.keio.ac.jp.

References

1. Banchereau J, Briere F, Caux C, et al. Immunobiology of dendritic cells. Annu Rev Immunol. 2000; 18:767-811.
2. Steinman RM, Hemmi H. Dendritic cells: translating innate to adaptive immunity. Curr Top Microbiol Immunol. 2006;311:17-58.
3. Takeda K, Kaisho T, Akira S. Toll-like receptors. Annu Rev Immunol. 2003;21:335-376.
4. Creagh EM, O'Neill LA. TLRs, NLRs and RLRs: a trinity of pathogen sensors that co-operate in innate immunity. Trends Immunol. 2006;27:352-357.
5. Trinchieri G. Interleukin-12 and the regulation of innate resistance and adaptive immunity. Nat Rev Immunol. 2003;3:133-146.
6. Vanhaesebroeck B, Leevers SJ, Ahmadi K, et al. Synthesis and function of 3-phosphorylated inositol lipids. Annu Rev Biochem. 2001;70:535-602.
7. Koyasu S. The role of PI3K in immune cells. Nat Immunol. 2003;4:313-319.
8. Fukao T, Tanabe M, Terauchi Y, et al. PI3K-mediated negative feedback regulation of IL-12 production in DCs. Nat Immunol. 2002;3:875-881.
9. Fukao T, Koyasu S. PI3K and negative regulation of TLR signaling. Trends Immunol. 2003;24:358-363.
10. Fukao T, Yamada T, Tanabe M, et al. Selective loss of gastrointestinal mast cells and impaired immunity in PI3K-deficient mice. Nat Immunol. 2002;3:295-304.
11. Goodridge HS, Harnett W, Liew FY, Harnett MM. Differential regulation of interleukin-12 p40 and p35 induction via Erk mitogen-activated protein kinase-dependent and -independent mechanisms and the implications for bioactive IL-12 and IL-23 responses. Immunology. 2003;109:415-425.
12. Martin M, Schifferle RE, Cuesta N, Vogel SN, Katz J, Michalek SM. Role of the phosphatidylinositol 3 kinase-Akt pathway in the regulation of IL-10 and IL-12 by Porphyromonas gingivalis lipopolysaccharide. J Immunol. 2003;171:717-725.
13. Kuo CC, Lin WT, Liang CM, Liang SM. Class I and III phosphatidylinositol 3′-kinase play distinct roles in TLR signaling pathway. J Immunol. 2006; 176:5943-5949.
14. Wullschleger S, Loewith R, Hall MN. TOR signaling in growth and metabolism. Cell. 2006;124: 471-484.
15. Suzuki H, Terauchi Y, Fujiwara M, et al. Xid-like immunodeficiency in mice with disruption of the p85alpha subunit of phosphoinositide 3-kinase. Science. 1999;283:390-392.
16. Terauchi Y, Tsuji Y, Satoh S, et al. Increased insulin sensitivity and hypoglycaemia in mice lacking the p85 alpha subunit of phosphoinositide 3-kinase. Nat Genet. 1999;21:230-235.
17. Takeda K, Clausen BE, Kaisho T, et al. Enhanced Th1 activity and development of chronic enterocolitis in mice devoid of Stat3 in macrophages and neutrophils. Immunity. 1999; 10:39-49.
18. Clausen BE, Burkhardt C, Reith W, Renkawitz R,

Forster I. Conditional gene targeting in macrophages and granulocytes using LysMcre mice. Transgenic Res. 1999;8:265-277.

19. Suzuki A, Yamaguchi MT, Ohteki T, et al. T cell-specific loss of Pten leads to defects in central and peripheral tolerance. Immunity. 2001;14:523-534.
20. Miyoshi H, Blomer U, Takahashi M, Gage FH, Verma IM. Development of a self-inactivating lentivirus vector. J Virol. 1998;72:8150-8157.
21. Nagai T, Ibata K, Park ES, Kubota M, Mikoshiba K, Miyawaki A. A variant of yellow fluorescent protein with fast and efficient maturation for cell-biological applications. Nat Biotechnol. 2002;20:87-90.
22. Suzue K, Kobayashi S, Takeuchi T, Suzuki M, Koyasu S. Critical role of dendritic cells in determining the Th1/Th2 balance and the disease outcome upon *Leishmania major* infection. Int Immunol. 2008;20:337-343.
23. Cross DA, Alessi DR, Cohen P, Andjelkovich M, Hemmings BA. Inhibition of glycogen synthase kinase-3 by insulin mediated by protein kinase B. Nature. 1995;378:785-789.
24. Guha M, Mackman N. The phosphatidylinositol 3-kinase-Akt pathway limits lipopolysaccharide activation of signaling pathways and expression of inflammatory mediators in human monocytic cells. J Biol Chem. 2002;277:32124-32132.
25. Yu Y, Nagai S, Wu H, Neish AS, Koyasu S, Gewirtz AT. TLR5-mediated phosphoinositide 3-kinase activation negatively regulates flagellin-induced proinflammatory gene expression. J Immunol. 2006;176:6194-6201.
26. Bierer BE, Mattila PS, Standaert RF, et al. Two distinct signal transmission pathways in T lymphocytes are inhibited by complexes formed between an immunophilin and either FK506 or rapamycin. Proc Natl Acad Sci U S A. 1990;87:9231-9235.
27. Long X, Lin Y, Ortiz-Vega S, Yonezawa K, Avruch J. Rheb binds and regulates the mTOR kinase. Curr Biol. 2005;15:702-713.
28. Moore KW, de Waal Malefyt R, Coffman RL, O'Garra A. Interleukin-10 and the interleukin-10 receptor. Annu Rev Immunol. 2001;19:683-765.
29. Ding Y, Chen D, Tarcsafalvi A, Su R, Qin L, Bromberg JS. Suppressor of cytokine signaling 1 inhibits IL-10-mediated immune responses. J Immunol. 2003;170:1383-1391.
30. Martin M, Rehani K, Jope RS, Michalek SM. Toll-like receptor-mediated cytokine production is differentially regulated by glycogen synthase kinase 3. Nat Immunol. 2005;6:777-784.
31. Rodionova E, Conzelmann M, Maraskovsky E, et al. GSK-3 mediates differentiation and activation of proinflammatory dendritic cells. Blood. 2007; 109:1584-1592.
32. Mocellin S, Marincola FM, Young HA. Interleukin-10 and the immune response against cancer: a counterpoint. J Leukoc Biol. 2005;78:1043-1051.
33. McGuirk P, McCann C, Mills KH. Pathogen-specific T regulatory 1 cells induced in the respiratory tract by a bacterial molecule that stimulates interleukin 10 production by dendritic cells: a novel strategy for evasion of protective T helper type 1 responses by Bordetella pertussis. J Exp Med. 2002;195:221-231.
34. Akbari O, DeKruyff RH, Umetsu DT. Pulmonary dendritic cells producing IL-10 mediate tolerance induced by respiratory exposure to antigen. Nat Immunol. 2001;2:725-731.
35. Lee YR, Yang IH, Lee YH, et al. Cyclosporin A and tacrolimus, but not rapamycin, inhibit MHC-restricted antigen presentation pathways in dendritic cells. Blood. 2005;105:3951-3955.
36. Hackstein H, Taner T, Zahorchak AF, et al. Rapamycin inhibits IL-4-induced dendritic cell maturation in vitro and dendritic cell mobilization and function in vivo. Blood. 2003;101:4457-4463.
37. Foster DA. Regulation of mTOR by phosphatidic acid? Cancer Res. 2007;67:1-4.
38. Puig-Kroger A, Relloso M, Fernandez-Capetillo O, et al. Extracellular signal-regulated protein kinase signaling pathway negatively regulates the phenotypic and functional maturation of monocyte-derived human dendritic cells. Blood. 2001; 98:2175-2182.
39. Kim AH, Khursigara G, Sun X, Franke TF, Chao MV. Akt phosphorylates and negatively regulates apoptosis signal-regulating kinase 1. Mol Cell Biol. 2001;21:893-901.
40. Cao X, Wei G, Fang H, et al. The inositol 3-phosphatase PTEN negatively regulates Fc gamma receptor signaling, but supports Toll-like receptor 4 signaling in murine peritoneal macrophages. J Immunol. 2004;172:4851-4857.
41. Park HS, Kim MS, Huh SH, et al. Akt (protein kinase B) negatively regulates SEK1 by means of protein phosphorylation. J Biol Chem. 2002;277: 2573-2578.
42. Utsugi M, Dobashi K, Ishizuka T, et al. c-Jun N-terminal kinase negatively regulates lipopolysaccharide-induced IL-12 production in human macrophages: role of mitogen-activated protein kinase in glutathione redox regulation of IL-12 production. J Immunol. 2003;171:628-635.
43. Ma W, Gee K, Lim W, et al. Dexamethasone inhibits IL-12p40 production in lipopolysaccharide-stimulated human monocytic cells by down-regulating the activity of c-Jun N-terminal kinase, the activation protein-1, and NF-kappa B transcription factors. J Immunol. 2004;172:318-330.
44. Gautier G, Humbert M, Deauvieau F, et al. A type I interferon autocrine-paracrine loop is involved in Toll-like receptor-induced interleukin-12p70 secretion by dendritic cells. J Exp Med. 2005;201: 1435-1446.
45. Hoentjen F, Sartor RB, Ozaki M, Jobin C. STAT3 regulates NF-κB recruitment to the IL-12p40 promoter in dendritic cells. Blood. 2005;105: 689-696.
46. Jefferies HB, Fumagalli S, Dennis PB, Reinhard C, Pearson RB, Thomas G. Rapamycin suppresses 5'TOP mRNA translation through inhibition of p70s6k. EMBO J. 1997;16:3693-3704.
47. Soliman GA. The mammalian target of rapamycin signaling network and gene regulation. Curr Opin Lipidol. 2005;16:317-323.
48. Cunningham JT, Rodgers JT, Arlow DH, Vazquez F, Mootha VK, Puigserver P. mTOR controls mitochondrial oxidative function through a YY1-PGC-1alpha transcriptional complex. Nature. 2007; 450:736-740.

THE JOURNAL OF BIOLOGICAL CHEMISTRY VOL. 283, NO. 20, pp. 14041–14052, May 16, 2008

A Novel GDP-dependent Pyruvate Kinase Isozyme from *Toxoplasma gondii* Localizes to Both the Apicoplast and the Mitochondrion*

Received for publication, November 2, 2007, and in revised form, March 3, 2008 Published, JBC Papers in Press, March 6, 2008, DOI 10.1074/jbc.M709015200

Tomoya Saito[‡1], Manami Nishi[§1], Muoy I. Lim[§], Bo Wu[§], Takuya Maeda[‡], Hisayuki Hashimoto[‡], Tsutomu Takeuchi[‡], David S. Roos[§2], and Takashi Asai[‡3]

From the [‡]Department of Tropical Medicine and Parasitology, Keio University School of Medicine, 35 Shinanomachi, Shinjuku-ku, Tokyo 160-8582, Japan and the [§]Department of Biology, University of Pennsylvania, Philadelphia, Pennsylvania 19104

We previously reported a cytosolic pyruvate kinase (EC 2.7.1.40) from *Toxoplasma gondii* (*Tg*PyKI) that differs from most eukaryotic pyruvate kinases in being regulated by glucose 6-phosphate rather than fructose 1,6-diphosphate. Another putative pyruvate kinase (*Tg*PyKII) was identified from parasite genome, which exhibits 32% amino acid sequence identity to *Tg*PyKI and retains pyruvate kinase signature motifs and amino acids essential for substrate binding and catalysis. Whereas *Tg*PyKI is most closely related to plant/algal enzymes, phylogenetic analysis suggests a proteobacterial origin for *Tg*PyKII. Enzymatic characterization of recombinant *Tg*PyKII shows a high pH optimum at 8.5, and a preference for GDP as a phosphate recipient. Catalytic activity is independent of K^+, and no allosteric or regulatory effects were observed in the presence of fructose 1,6-diphosphate, fructose 2,6-diphosphate, glucose 6-phosphate, ribose 5-phosphate, AMP, or ATP. Unlike *Tg*PyKI, native *Tg*PyKII activity was exclusively associated with the membranous fraction of a *T. gondii* tachyzoite lysate. *Tg*PyKII possesses a long N-terminal extension containing five putative start codons before the conserved region and localizes to both apicoplast and mitochondrion by immunofluorescence assay using native antibody and fluorescent protein fusion to the N-terminal extension. Further deletional and site-directed mutagenesis suggests that a translation product from 1st Met is responsible for the localization to the apicoplast, whereas one from 3rd Met is for the mitochondrion. This is the first study of a potential mitochondrial pyruvate kinase in any system.

Toxoplasma gondii is an obligate intracellular protozoan parasite of warm-blooded animals, including humans (1). Although normally asymptomatic, toxoplasmosis is a significant problem in pregnant women infected early during gestation, immunocompromised individuals, and livestock. This parasite is a member of the phylum Apicomplexa, which includes many other parasites such as *Plasmodium* species responsible for malaria. Glucose is thought to be the main source of energy for the rapidly multiplying forms of both *Toxoplasma* and *Plasmodium*, which use the Embden-Meyerhof pathway for glycolytic phosphorylation (2).

Pyruvate kinase catalyzes the essentially irreversible transphosphorylation from phosphoenolpyruvate (PEP)[4] to ADP-producing pyruvate (3). In most mammals and bacteria, pyruvate kinase is allosterically regulated by fructose 1,6-diphosphate (4) and thus plays a regulatory role in glycolysis. The product pyruvate feeds into many metabolic pathways, placing pyruvate kinase at a crucial metabolic intersection. Many organisms express multiple pyruvate kinase isozymes with different kinetic properties. For example, *Escherichia coli* bears two isozymes, type I and II, both of which are homotropically activated by the substrate PEP. The type I isozyme is also activated heterotropically by fructose 1,6-diphosphate and is inhibited by ATP (5), whereas the type II isozyme is activated by AMP and monophosphorylated sugars (6). Pyruvate kinases are expressed in the cytosol in most organisms. Plants and algae have additional isozymes in chloroplasts with markedly different physical and kinetic/regulatory characteristics (7).

We have previously described the kinetic and regulatory properties of the cytosolic *T. gondii* pyruvate kinase (*Tg*PyKI). Unlike *T. gondii* hexokinase (8) and phosphofructokinase (9) that lack allosteric regulation, *Tg*PyKI is allosterically regulated by glucose 6-phosphate (10, 11), suggesting an important role in the control of glycolysis. We recently identified a second,

* This work was supported, in whole or in part, by National Institutes of Health grants. This work was also supported by Grant-in-aid for Scientific Research (KAKENHI) for Young Scientists (B) from the Ministry of Education, Culture, Sports, Science, and Technology 15790217, a Keio University grant-in-aid for encouragement of young medical scientists, and a Keio University special grant-in-aid for innovative collaborative research projects. The costs of publication of this article were defrayed in part by the payment of page charges. This article must therefore be hereby marked "*advertisement*" in accordance with 18 U.S.C. Section 1734 solely to indicate this fact.

The nucleotide sequence(s) reported in this paper has been submitted to the GenBank™/EBI Data Bank with accession number(s) AB118155.

[1] Both authors contributed equally to this work.

[2] Senior Scholar in Global Infectious Diseases of the Ellison Medical Foundation.

[3] To whom correspondence should be addressed: Dept. of Tropical Medicine and Parasitology, Keio University School of Medicine, 35 Shinanomachi, Shinjuku-ku, Tokyo 160-8582, Japan. Tel.: 81-3-3353-1211 (Ext. 62747); Fax: 81-3-3353-5958; E-mail: asait@sc.itc.keio.ac.jp.

[4] The abbreviations used are: PEP, phosphoenolpyruvate; ACP, acyl carrier protein; *Tg*PyK, *T. gondii* pyruvate kinase; YFP, yellow fluorescent protein; SA, predicted signal anchor; SP signal peptide; pTP, predicted plastid transit peptide; mTP, predicted mitochondrion targeting peptide; aa, amino acid; CHES, 2-(cyclohexylamino)ethanesulfonic acid; bis-Tris, 2-[bis(2-hydroxyethyl)amino]-2-(hydroxymethyl)propane-1,3-diol; MOPS, 4-morpholinepropanesulfonic acid; PBS, phosphate-buffered saline; Ab, antibody; HA, hemagglutinin; MES, 2-(*N*-morpholino)ethanesulfonic acid; HFF, human foreskin fibroblast; IFA, immunofluorescence assay; ER, endoplasmic reticulum; TES, 2-[[2-hydroxy-1,1-bis(hydroxymethyl)ethyl]amino]ethanesulfonic acid; NDP, nucleoside diphosphate; RFP, red fluorescent protein.

highly diverged isozyme in *T. gondii* EST and genome data bases (12, 13). This study describes the molecular genetic characterization, phylogeny, recombinant expression/purification, kinetic characterization, and subcellular localization of this *T. gondii* pyruvate kinase isozyme (*Tg*PyKII).

EXPERIMENTAL PROCEDURES

Parasites, Host Cells, Chemicals, and Reagents—RH strain *T. gondii* tachyzoites were maintained by serial passage in primary human foreskin fibroblasts (HFF) in Eagle's minimum essential media (Invitrogen) containing 1% heat-inactivated fetal bovine serum (Ed1 media) (14) or in mouse peritoneal fluid (15). Construction of parasites stably expressing p*tub*FNR$_L$-yellow fluorescent protein (YFP)-HA (labeling the apicoplast) and p*tub*HSP60$_L$-RFP (labeling the mitochondrion) is described elsewhere (16). PEP, phosphorylated sugars, nucleotides, potassium ferricyanide, and amino acids were obtained from Sigma. Rabbit polyclonal anti-acyl carrier protein (ACP) antibody was kindly provided by Drs. G. I. McFadden and R. F. Waller (17). MitoTrackerRed CMXRos (8-(4′-chloromethyl) phenyl-2,3,5,6,11,12,14,15-octahydro-1*H*,4*H*,10*H*,13*H*-diquinolizino-8*H*-xanthylium chloride), and Alexa Fluor Marina Blue/361 and 594-conjugated goat anti-rabbit antibodies were obtained from Invitrogen.

Cloning and Sequencing of TgPyKII cDNA—The following PCR primers were designed based on *T. gondii* ESTs CB030989, CB030879, and BI921053 (8): 5′-TGCAGAAATCGTCGCGCCGCAGCG-3′ (sense) and 5′-GCCGTGCTTGCCTTCTTTGG-3′ (antisense). PCR amplification of a *T. gondii* RH tachyzoite λZAP-II cDNA library (kindly provided by Dr. J. Ajioka, Cambridge University, UK) yielded a product with the expected size of 371 bp, which was used as a probe for cDNA library screening (8). Positive clones were sequenced on both strands using a Genetic Analyzer model 310 and 3700 (Applied Biosystems, Tokyo, Japan). The composite cDNA sequence was used for BLAST query against ToxoDB (18) to identify gene model TgTigrScan_6611. To confirm the 5′ end of the *Tg*PyKII cDNA, total RNA was extracted from RH strain of *T. gondii* tachyzoites (RNAqueous, Ambion, TX), and cDNA was amplified using GeneRacer kit (Invitrogen). 5′-rapid amplification of cDNA ends was performed using a gene-specific primer 5′-CACGTAGACAGAGGTGACGCTTCGGGG-3′. The complete cDNA sequence was analyzed by VectorNTI software (InforMax, Bethesda). The protein domains, families, and functional sites were analyzed using PROSITE (19). Signal properties were analyzed using TargetP (20, 21), SignalP (21, 22), and ChloroP (23) softwares. Hydrophobicity was examined using the Kyte and Doolittle procedure (24).

Phylogenetic Analysis—Twenty nine pyruvate kinase sequences from 20 taxa were extracted from GenBank™ and the OrthoMCL data base (25, 26) (see Fig. 2 legend for GenBank™ accession number), and aligned using ClustalX 1.83 (27), with manual curation. Regions of uncertain alignment were omitted, leaving 333 amino acid positions for analysis. Maximum likelihood trees were constructed using PROML from the PHYLIP 3.6a3 package (28), with 100 replicates, global rearrangement, and randomized input order options in conjunction with estimated parameter γ and the proportion of invariable sites obtained from TREE-PUZZLE5.1 (29). Bayesian analysis (30, 31) was carried out using MrBayes 3.0 with the JTT amino acid substitution model and 200,000 search generations.

Expression and Purification of Recombinant TgPyKII—An open reading frame predicted to encode the conserved region (from amino acid 293 to 988) of *Tg*PyKII was amplified using primers 5′-TACGGATCCCTCTCTGCTGCGTCGCCC-3′ (sense) and 5′-TCGGGATCCCTATCGCCCTGACTCGAGAGT-3′ (antisense), and cloned into the BamHI site of vector pGEX-6p-1 (Amersham Biosciences). Expression of the glutathione *S*-transferase-*Tg*PyKII-(293–988) fusion protein in *E. coli* BL21 was induced with 0.5 mM isopropyl β-thiogalactoside for 2.5 h, and purification of recombinant *Tg*PyKII was carried out by affinity chromatography on glutathione-Sepharose 4B (Amersham Biosciences), followed by treatment with PreScission Protease (Amersham Biosciences). The protein was applied to a DEAE-Toyo Pearl 650s column (TOSOH, Tokyo, Japan) equilibrated with 10 mM Tris-Cl, pH 8.0, containing 1 mM EDTA. Peak fractions eluted with a linear 0–500 mM gradient of KCl were pooled, concentrated, assayed for purity and concentration, and stored in 30% glycerol (w/v) at −80 °C. The protein concentration was determined by the dye-binding procedure described by Bradford (32) using bovine serum albumin as a standard. The purity of recombinant pyruvate kinase was analyzed by electrophoresis on 5–10% acrylamide gel. The protein was detected by Coomassie Brilliant Blue R-250 staining.

Enzyme Assays—Pyruvate kinase activity was determined by lactate dehydrogenase-coupled spectrophotometric assay (32), whereas monitoring oxidation of NADH due to pyruvate reduction at 340 nm was by using a UV-1600 spectrophotometer equipped with a TCC-240A temperature-controlled cell (Shimazu Co, Kyoto, Japan). 1-ml standard reaction mixture for assaying *Tg*PyKII activity contained 1 mM PEP, 0.5 mM GDP, 25.5 mM $MgCl_2$, 0.2 mM NADH, 20 units of rabbit muscle lactate dehydrogenase type II (Sigma), 100 mM Tris-Cl, pH 8.5, and 10–20 ng of the test enzyme. For substrate specificity studies, $MgCl_2$ was added in 25 mM excess of NDP to ensure formation of the $MgNDP^{2-}$ complex. All reactions were initiated by the addition of the substrate NDP. For determining optimal pH of recombinant *Tg*PyKII, MES, Tris-Cl, or CHES/NaOH buffers were used to generate a pH range from 6.0 to 10.0. Activities of *Tg*PyKI and succinate dehydrogenase were assayed as described previously (10, 11). All assays were carried out in triplicate at 37 °C. Reactions were monitored for 5 min, and the initial velocity was calculated from a tangent fitted to the reaction curve. Kinetic data were calculated using a nonlinear curve fitting algorithm (SigmaPlot 2000 software; SPSS Inc., Chicago).

Subcellular Fractionation of T. gondii Tachyzoites—10^{10} tachyzoites were washed twice and resuspended in TES homogenization buffer (250 mM sucrose, 1 mM EDTA, 5 mM triethanolamine-HCl, pH 7.5) and disrupted by French press at 35 kg/cm^2. After sedimentation of unbroken cells (~10%) at 2250 × *g* for 10 min, the supernatant was centrifuged for 20 min at 20,000 × *g* to yield a cytosolic (supernatant) and membranous (pellet) fractions. The pellet was washed once, resuspended in 1% Triton X-100 in TES buffer, and mechanically homogenized using a polychlorotrifluoroethylene homogenizer.

Native Antibody Production and Immunoblotting—Recombinant *Tg*PyKII-(293–988) purified from *E. coli* was used to immunize New Zealand White rabbits. Following three 50-μg injections at 2-week intervals, whole IgG was isolated from serum, and anti-*Tg*PyKII IgG was affinity-purified using CNBr-activated Sepharose 4B (Amersham Biosciences), which couples recombinant *Tg*PyKII-(293–988) as described previously (33). To check the cross-reactivity of anti-*Tg*PyKII to *Tg*PyKI, 3 ng of recombinant *Tg*PyKI (11) and recombinant *Tg*PyKII were loaded on 8% gradient polyacrylamide gel, which was then transferred to a Nitrocellulose Hybond-C extra membrane (Amersham Biosciences) using a semidry blotting apparatus. The membrane was blocked for 20 min with 2% skimmed milk in phosphate-buffered saline (PBS) containing 0.2% Tween 20 and incubated for 1 h with anti-*Tg*PyKII antibody (1:25 in blocking solution). Following washes in PBS with 0.2% Tween 20, the membrane was incubated with alkaline phosphatase goat anti-rabbit IgG (1:3000) (Vector Laboratories) for 1 h, following detection with a 5-bromo-4-chloro-3-indolyl phosphate-nitro blue tetrazolium system (Roche Applied Science). The molecular sizes of protein bands were determined with reference to pre-stained SDS-gel electrophoresis standards (Bio-Rad). To detect endogenous *Tg*PyKII expressed in *T. gondii*, 10^8 RH tachyzoites released from HFF monolayer were filtered through 3-μm pore-size Nuclepore polycarbonate filters (Whatman) and pelleted by centrifugation at 900 × *g* for 12 min. Parasites were lysed in PBS, containing NuPAGE LDS sample buffer (Invitrogen) and 0.5 M dithiothreitol. After denaturation at 70 °C for 10 min, parasite lysates were loaded on bis-Tris, 4–12% polyacrylamide gels (Invitrogen), and protein gel electrophoresis was performed using NuPAGE system with MOPS/SDS running buffer (Invitrogen). Proteins were transferred to nitrocellulose membrane using a Trans-Blot SemiDry apparatus (Bio-Rad), which was then blocked with 5% nonfat dry milk and 3% fetal bovine serum in PBS. The membrane was incubated for 1 h with a rabbit anti-*Tg*PyKII Ab (1:25 dilution) in blocking solution containing 0.2% Tween 20 (Sigma). Following washes in PBS with 0.2% Tween 20, the membrane was incubated for 1 h with a horseradish peroxidase-conjugated goat anti-rabbit secondary antibody (Bio-Rad) (1:2500 dilution) in blocking solution containing 0.2% Tween 20. Chemiluminescence reaction was performed using ECL Western blotting detection reagents (Amersham Biosciences), and blots were exposed on Kodak BioMax film.

Plasmid Construction—N-terminal 357 amino acids of *Tg*PyKII (unconserved region containing five possible start codons) from 1st Met were amplified from a *T. gondii* RH cDNA using primers (note that restriction enzyme site is underlined and start codon is boldface) 5′-CATCGCAGATCT**ATG**GACGATGGTGGAGCAGAGT-3′ (sense) and 5′-CGTCACACTAGTCGGTCCGATGGTTGC-3′ (antisense) and subcloned into BglII/AvrII sites of the *T. gondii* expression vector p*tub* or p*min*PT_F-YFP-HA (16)[5] to produce p*tub*/p*min*Tg PyKII1stM-(1–357)-YFP-HA. DNA fragments from each downstream four start codons were generated using p*tub*/p*min*Tg PyKII1stM-(1–357)-YFP-HA as a template, the above antisense primer, and the following sense primers: 5′-CATCGCAGATCT**ATG**AACTTTCCAACTTGT-3′ (from 2nd Met); 5′-CATCGCAGATCT**ATG**GCGCCTCTCCGACCC-3′ (from 3rd Met); 5′-CATCGCAGATCT**ATG**GATTTTCCACGGGTG-3′ (from 4th Met); or 5′-CATCGCAGATCT**ATG**CTCTCTGCTGCGTCG-3′ (from 5th Met). Plasmids p*tub*/p*min*Tg PyKII2ndM-(19–357)-YFP-HA, p*tub*/p*min*Tg PyKII3rdM-(93–357)-YFP-HA, p*tub*/p*min*Tg PyKII4thM-(122–357)-YFP-HA, and p*tub*/p*min*Tg PyKII5thM-(293–357)-YFP-HA were constructed using above described subcloning method. To introduce a point mutation, methionine to alanine, at 2nd or 3rd Met, site-directed mutagenesis was performed using QuikChange site-directed mutagenesis kit (Stratagene, CA). The plasmid p*tub*/p*min*PyKII1stM-(1–357)-YFP-HA was used as a template in the PCR by utilizing the following sets of primers (mutated amino acids are lowercase): 5′-GCTAATGGTTTTGCCAGCgcGAACTTTCCAACTTGTGG-3′ and 5′-CCACAAGTTGGAAAGTTCgcGCTGGCAAAACCATTAGC-3′ to produce p*tub*/*min*PyKII[2ndM19A]-YFP-HA, and 5′-CTCCTTCTCTCCGCGgcGGCGCCTCTCCGACC-3′ and 5′-GGTCGGAGAGGCGCCgcCGCGGAGAGAAGGAG-3′ to produce p*tub*/*min*PyKII[3rdM93A]-YFP-HA.

Parasite Transfection, Immunofluorescence Assay, and Fluorescent Microscopy—Parasite transfection was performed by electroporation as described previously (14). Parasites were inoculated onto glass coverslips (22 mm in diameter) with a confluent monolayer of HFF cells and incubated in a humidified 37 °C incubator for 24 h. Following a wash with PBS, coverslips were fixed with 3.7% paraformaldehyde in PBS, pH 7.0, for 5 min, permeabilized with 0.25% Triton X-100 in PBS, pH 7.0, for 10 min, and blocked for 30 min in a blocking solution (3% bovine serum albumin (fraction V, Fisher) and 5% fetal bovine serum in PBS, pH 7.0). For MitoTracker labeling, coverslips were incubated with 150 nM MitoTrackerRed CMXRos (Invitrogen) for 30 min and washed twice with Ed1 media before fixation. For immunofluorescence assay (IFA), coverslips were incubated with primary antibodies (anti-*Tg*PyKII Ab at 1:25 dilution or anti-ACP Ab at a 1:2000 dilution in blocking solution) for 1 h. Coverslips were washed three times with 0.25% Triton X-100 in PBS, and primary antibodies were detected either with Alexa Fluor Marina Blue/361-conjugated (1:500 dilution) or 594-conjugated goat anti-rabbit antibodies (1:4000 dilution) (Invitrogen) in the blocking solution for 1 h. After two washes with 0.25% Triton X-100 in PBS and a wash with PBS, the coverslips were mounted on glass slides using Fluoromount-G (SouthernBiotech, AL). To find out the localization of endogenous *Tg*PyKII, parasites stably expressing FNR_L-YFP-HA were labeled with MitoTracker Red CMXRos and subjected to IFA using anti-*Tg*PyKII and Alexa Fluor Marina Blue/361-conjugated goat anti-rabbit antibodies (Invitrogen). For examination of deletional constructs, wild type RH parasites were transfected, labeled with MitoTracker Red CMXRos, and subjected to IFA with anti-ACP and Alexa Fluor Marina Blue/361-conjugated goat anti-rabbit antibodies. Point mutational constructs were transfected either to wild type RH parasites that are subsequently labeled with anti-ACP and Alexa Fluor 594-conjugated goat anti-rabbit antibodies (Invitrogen) or to parasites stably expressing p*tub*$HSP60_L$-RFP.

[5] M. Nishi, C. He, O. Harb, J. Murray, and D. Roos, manuscript in preparation.

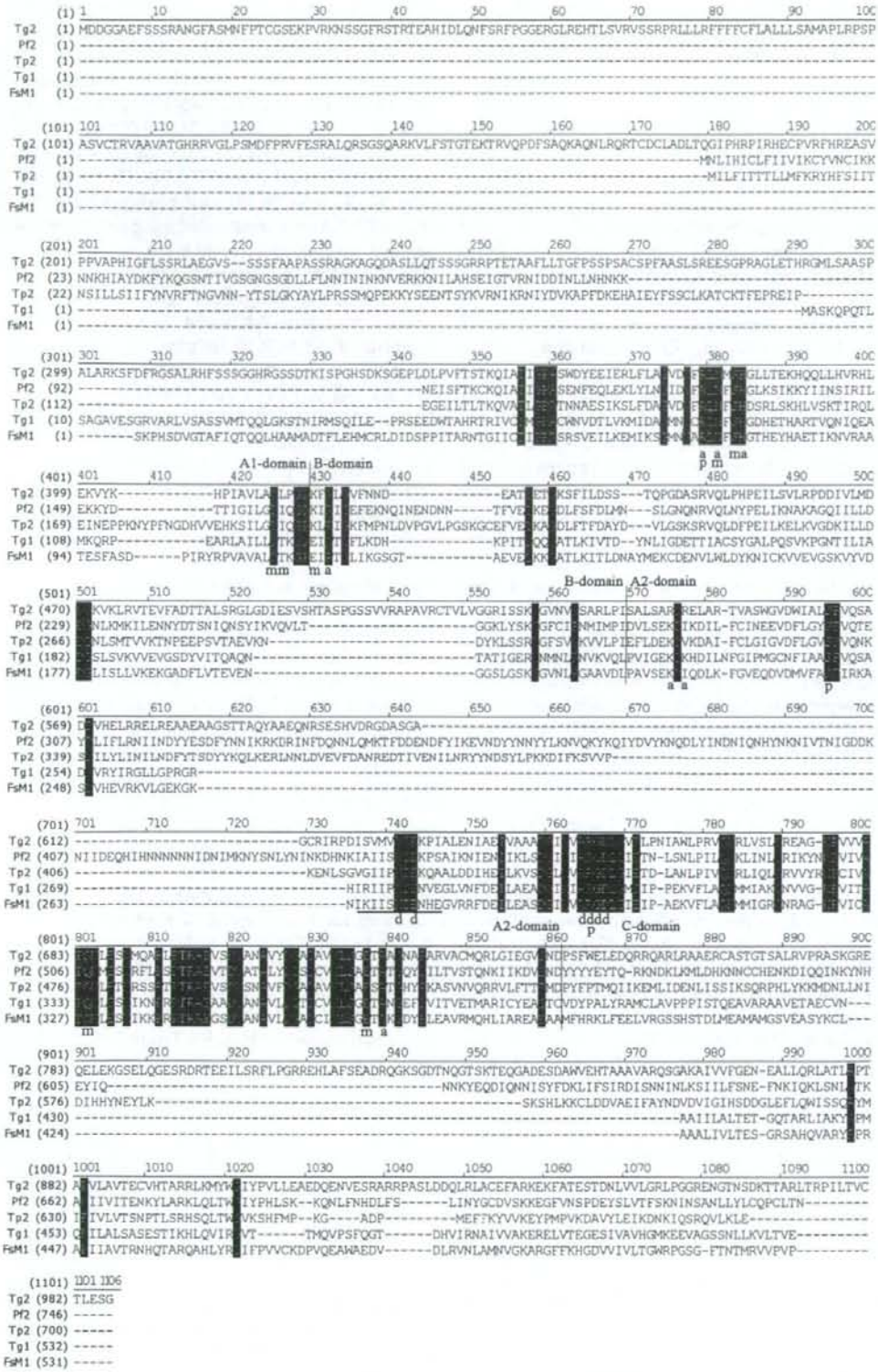
A1-domain
B-domain
B-domain
A2-domain
A2-domain
C-domain
Tg2
Pf2
Tp2
Tg1
FsM1

Stacked images were collected using an Olympus IX70 inverted microscope equipped with a 100-watt Hg-vapor lamp with appropriate barrier/emission filters. Images were captured with a CoolSNAP Hi Res CCD camera (Photometrics, AZ) and DeltaVision softWoRx software (Applied Precision, WA). All images were subjected to three-dimensional rendering using DeltaVision softWoRx.

RESULTS

Gene Organization, Functional Motifs, and Phylogenetic Analysis of TgPyKII—We cloned a second pyruvate kinase isozyme gene from *T. gondii*, *Tg*PyKII, using EST data bases, cDNA library screening, and rapid amplification of cDNA ends. A BLAST search of the cDNA sequence in ToxoDB (18) identified the gene model TgTigrScan_6611 in chromosome III, consisting of two exons (1092 and 1871 bp) and an intron (764 bp) that encodes 988 amino acids with a calculated molecular mass of 106,837 Da and a pI of 8.77. BLASTP search shows that *Tg*PyKII is highly homologous to pyruvate kinases from α-proteobacteria with >40% identity and >50% similarity. Multiple sequence alignments with crystallized pyruvate kinases (35–37) show that *Tg*PyKII has a long N-terminal extension before the conserved region beginning at aa 345 (Fig. 1).

Compared with the pyruvate kinase domain structure consisting of A_1, A_2, B, and C domains, three unique insertions in the middle of domain B, A_2, and C (37), are present (Fig. 1). Both *Tg*PyKI and *Tg*PyKII contain a pyruvate kinase signature (PROSITE; PS00110) (Fig. 1, *line*) as well as consensus motifs for pyruvate kinase, including binding sites of ADP, PEP, and divalent cations (Fig. 1, *a*, *p*, *d*, respectively). *Tg*PyKI possesses all the conserved monovalent cation-binding sites (Fig. 1, *m*). In contrast, in *Tg*PyKII, two binding sites Thr^{113} and Glu^{117} in *Felis catus* pyruvate kinase are substituted by Leu^{412} and Lys^{416}, respectively. These substitutions are a common feature of monovalent cation-independent pyruvate kinases (38–40). Furthermore, the presence of Glu^{868} in *Tg*PyKII, conserved among enzymes that are insensitive to the pyruvate kinase activator, fructose 1,6-diphosphate (39), suggests that *Tg*PyKII is not activated by fructose 1,6-diphosphate.

*Tg*PyKII has overall amino acid sequence identity of 32% to *Tg*PyKI. Unlike *Tg*PyKII, *Tg*PyKI shows high homology to pyruvate kinases in other apicomplexan parasites and plants. Phylogenetic tree indicates that *Tg*PyKI is closely related to plant cytosolic pyruvate kinases along with pyruvate kinases from apicomplexan parasites such as *Cryptosporidium parvum* (EAK88569), *Plasmodium falciparum* (CAG25081), and *Theileria parva* (529.m04777) (Fig. 2). In contrast, *Tg*PyKII clusters with proteobacteria pyruvate kinases, along with two isozymes from apicomplexan parasites *P. falciparum* (AAG35560) and *T. parva* (529.m04771) (Fig. 2). These results suggest a different evolutionary origin of the two isozymes in *T. gondii*, a probable plant/algal origin of *Tg*PyKI and a probably proteobacterial origin of *Tg*PyKII.

Enzymatic Activity of Recombinant and Native TgPyKII Proteins—Conserved region of *Tg*PyKII (*Tg*PyKII-(293–988)) was expressed in *E. coli* as a fusion protein with glutathione *S*-transferase, which was removed by PreScission protease (Amersham Biosciences) digestion. SDS-PAGE detected the predicted size of 77 kDa for purified recombinant protein (Fig. 3*A*). The purified recombinant protein is shown to catalyze the pyruvate kinase reaction. The pH optimum of *Tg*PyKII activity is at pH 8.5, and more than 80% of the maximal activity is observed between pH 8.0 and pH 9.5 (data not shown). At pH 7.0, the optimal pH of *Tg*PyKI (11), the activity of *Tg*PyKII is 50% of the maximal activity. The enzyme was stable when stored in buffer containing 20 mM Tris-Cl, pH 7.0, and 30% glycerol for 1 week at 4 °C. The enzyme activity remained stable after one freeze-thaw cycle.

Most pyruvate kinases require monovalent cations, show allosteric properties for PEP binding, and are regulated by phosphorylated sugars. Interestingly, amino acid sequence (Fig. 1) suggests that monovalent cations are not required for *Tg*PyKII activity, which was confirmed by biochemical assay. Also, the saturation curve is hyperbolic with the substrate PEP. The K_m value for PEP is 0.116 ± 0.011 mM. Although most pyruvate kinases prefer ADP as a phosphate recipient, the k_{cat}/K_m values for GDP and IDP are 337- and 114-fold higher, respectively, than that for ADP (Table 1). Moreover, the substrates GDP and IDP exert inhibitory activities (Table 1). The specific activity at 0.5 mM CDP and UDP was less than 10% that at 0.5 mM GDP. These data indicate that GDP is a preferred substrate for *Tg*PyKII. Other possible effectors were tested at sub-saturating concentrations of PEP and GDP (0.2 and 0.1 mM, respectively). None of the following compounds influence *Tg*PyKII activity: fructose 1,6-diphosphate, glucose 6-phosphate, fructose 6-phosphate, glucose 1-phosphate, ribose 5-phosphate, ATP, ITP, AMP, His, Ser, Ala, Glu, Gln, Thr, Met, Gly, Ile, Asn, Cys, Pro, Arg, Lys, Phe, Trp, Leu, Asp, Val (1 mM each), Tyr (0.5 mM), 0.1 mM acetyl-CoA. Only 0.1 mM GTP reduces the V_{max} by 10 ± 1%.

To examine native *Tg*PyKII activity, we performed subcellular fractions of *T. gondii* tachyzoite cells. *Tg*PyKI and -II activities were distinguished based on their pH optimum (7.0 *versus* 8.5, respectively), requirement for the monovalent cation, and phosphate recipient specificity (ADP *versus* GDP) (Table 2). As *Tg*PyKI requires K^+ for the activity, *Tg*PyKI does not show any activity in the standard assay condition for *Tg*PyKII lacking K^+. In the standard assay condition for *Tg*PyKI, *Tg*PyKII shows less than 1/100 of its *Tg*PyKII activity. Although *Tg*PyKI activity is detected only in cytosolic fractions as reported previously (10), *Tg*PyKII activity is exclusively associated with membranous

FIGURE 1. **Amino acid sequence alignment of *T. gondii* pyruvate kinase II with four pyruvate kinases from other species.** Accession numbers for the sequence data shown are as follow: *Tg2*, *T. gondii* isozyme II (this study; AB118155); *Pf2*, *P. falciparum* isozymes II (AAN35560); *Tp2*, *T. parva* isozyme II (529.m04771); *Tg1*, *T. gondii* isozymes I (BAB47171); *FsM1*, *F. catus* isozyme M1 (P11979). Identical residues are highlighted in *black*. *Vertical lines* indicate the dividing line of four three-dimensional domains (*N*, *A1*, *A2*, *B*, *C*) of pyruvate kinase as described previously (37). A *horizontal line* indicates the pyruvate kinase signature sequence (PROSITE, PS00110; *p* indicates PEP-binding sites; *a* indicates ADP-binding sites; *d* indicates divalent cation-binding sites; *m* indicates monovalent cation-binding sites; *dashes* indicates gaps in the alignment.

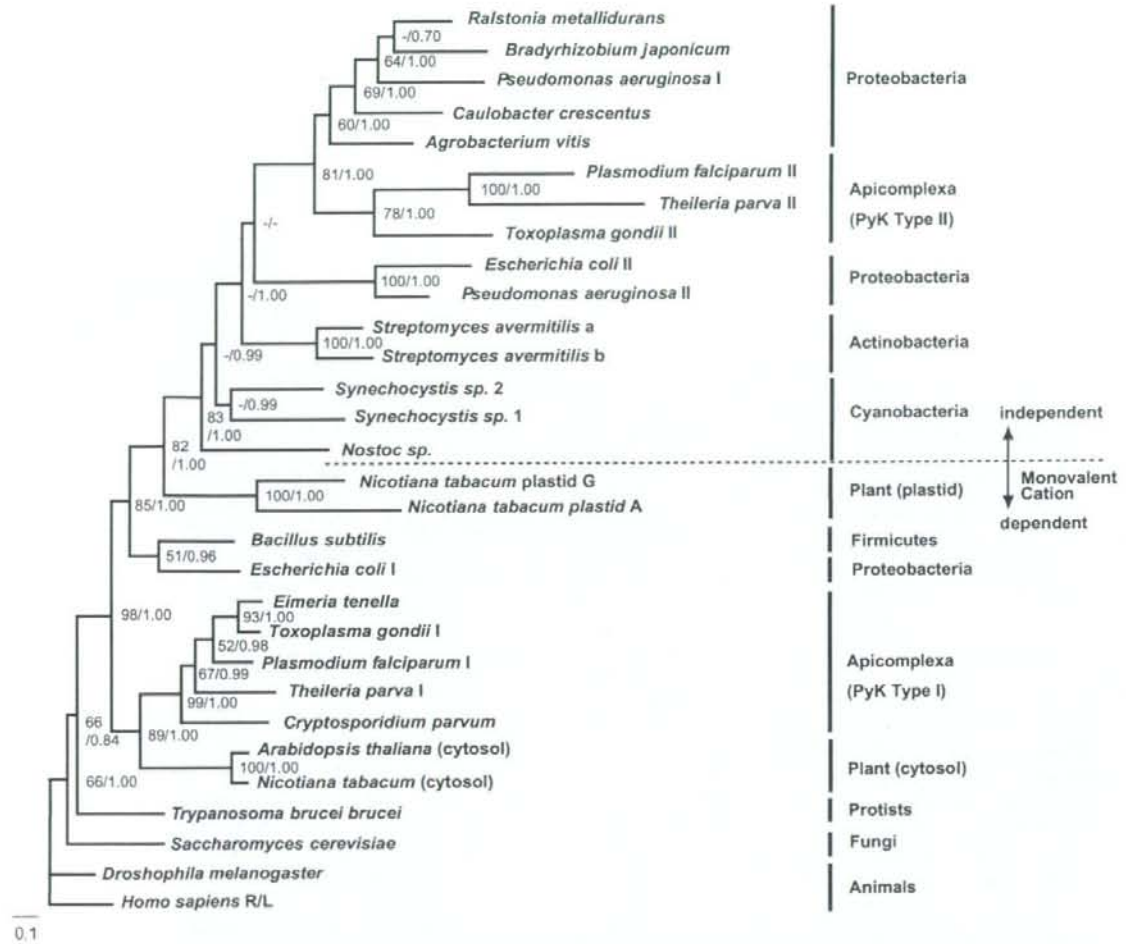

FIGURE 2. **Phylogenetic tree of pyruvate kinase constructed based on the deduced amino acid sequences of pyruvate kinase genes of 20 taxa.** Only evolutionarily conserved alignment regions (~230 amino acid characters) were used for phylogenetic inference by the Bayesian inference and maximum likelihood methods. The tree shown is the consensus tree estimated by Bayesian analysis with the JTT matrix. Maximum likelihood distance tree was also carried out. *Numbers* at branches are bootstrap values for the maximum likelihood protein distance analysis (100 replicates, >50 were indicated) and Bayesian posterior probabilities (>0.5 were indicated). *Bar* indicates the substitution. The accession numbers in GenBank™ for all pyruvate kinase sequences used for phylogenetic analysis are as follows: *Drosophila melanogaster* (AAC16244); *Homo sapiens* R/L (AAA60104);*Saccharomyces cerevisiae* (CAA32573); *Trypanosoma brucei brucei* (P30615); *C. parvum* (EAK88569); *P. falciparum* (I, CAG25081; II, AAN35560); *T. gondii* (I, BAB47171; II, in this article); *T. parva* (I, 529.m04777; II, 529.m04771); *A. thaliana* (cytosol, BAB10006); *Nicotiana tabacum* (cytosol, CAA82628; plastid A, CAA82222; plastid G, CAA82223); *Streptomyces avermitilis* (a, BAC70536; b, BAC73928);*Synechocystis* sp. (1, BAA10621; 2, BAA17574); *Nostoc* sp. PCC7120 (BAB74263); *Bacillus subtilis* (P80885); *E. coli* (type I, AAA24392; type II, AAA24473); *Pseudomonas aeruginosa* (I, NP_250189; II, NP_253019); *Bradyrhizobium japonicum* (NP_773778); *Ralstonia metallidurans* (ZP_00275735); *Caulobacter crescentus* (NP_420856); and *Agrobacterium vitis* (Q44473).

fraction, the purity of which is confirmed by mitochondrial succinate dehydrogenase activity. The procedure of solubilization of membranous fraction did not have any detrimental impact on the activity of recombinant *Tg*PyKII. Thus, *Tg*PyKII is localized to membrane-bound compartments.

Localization of TgPyKII and Analysis of Its Subcellular Localization Signals—Anti-*Tg*PyKII antibody was generated to detect endogenous *Tg*PyKII protein in *T. gondii* tachyzoite cells. Western blot analysis shows that anti-*Tg*PyKII antibody specifically detects the recombinant *Tg*PyKII protein (Fig. 3*B*, *lane 1*), not the recombinant *Tg*PyKI protein (Fig. 3*B*, *lane 2*) and the host cell (data not shown). A single band of ~75 kDa was detected by this antibody in whole lysate of tachyzoite cells (Fig. 3*C*). To analyze the localization of native *Tg*PyKII protein in tachyzoite cells, FNR_L-YFP-HA parasites (labeling the apicoplast) were labeled with MitoTracker Red (labeling the mitochondrion) and *Tg*PyKII antibody (Fig. 4). Endogenous *Tg*PyKII (Fig. 4, *blue*) localizes to the apicoplast (Fig. 4, *green*) and the mitochondrion (Fig. 4, *red*) along with apical side of endoplasmic reticulum (ER) (Fig. 4, *arrowheads*), which was confirmed with a co-localization experiment using ER marker (data not shown).

Multiple sequence alignments of pyruvate kinases (Fig. 1) show that *Tg*PyKII has a long N-terminal unconserved extension containing five possible start codons (Fig. 5*A*, *red bold*), which may acts as subcellular localization signal(s). TargetP,

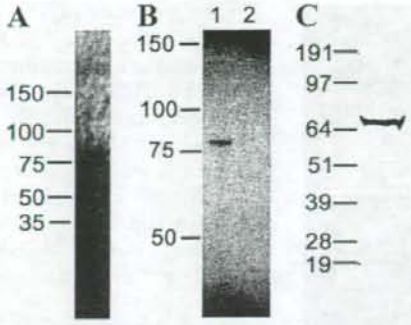

FIGURE 3. **Recombinant protein expression and native antibody of *Tg*PyKII.** *A*, SDS-PAGE of 3 μg of purified recombinant *Tg*PyKII with the N-terminal extension truncated. Electrophoresis was carried out on 5–10% gradient polyacrylamide gel. The protein was detected by Coomassie Brilliant Blue R-250 staining. *B* and *C*, specificity of anti-*Tg*PyKII IgG shown by Western blot analysis. *B*, 3 ng of recombinant *Tg*PyKII (*lane 1*) and *Tg*PyKI (*lane 2*). *C*, 1×10^8 *T. gondii* tachyzoite whole cell lysate. Molecular mass is expressed in kDa.

TABLE 1

Kinetic parameters of *T. gondii* pyruvate kinase I and II for nucleoside diphosphates

Substrate	Enzyme	K_m	K_i[a]	k_{cat}[b]	k_{cat}/K_m
		mM	mM	s^{-1}	$mM^{-1}\,s^{-1}$
ADP	*Tg*PyKI[c]	0.180 ± 0.110		174	966
	*Tg*PyKII[d]	7.99 ± 0.44		47.6 ± 1.4	6
GDP[e]	*Tg*PyKII	0.0544 ± 0.0061	1.68 ± 0.18	110 ± 4	2020
IDP[f]	*Tg*PyKII	0.193 ± 0.014	4.89 ± 0.49	131 ± 4	681

[a] GDP and IDP exhibited substrate inhibition.
[b] k_{cat} values were calculated as V_{max} divided by molar enzyme concentration.
[c] Cited and calculated from data in Maeda *et al.* (11).
[d] ADP concentration assayed was 1 to 10 mM.
[e] GDP concentration assayed was 0.025 to 2 mM.
[f] IDP concentration assayed was 0.05 to 4 mM.

TABLE 2

Total activity of enzymes in subcellular fractions of *T. gondii* tachyzoites

Fraction	Total activity[a] (units/10^{10} tachyzoite cells)		
	Pyruvate kinase activity		SDH[d]
	*Tg*PyKI[b]	*Tg*PyKII[c]	
Cytosolic fraction	153 ± 7	<0.01	<0.005
Membranous fraction	<0.01	0.920 ± 0.190	0.854 ± 0.088

[a] All values were determined by three independent experiments. One unit of enzyme activity is defined as the amount of enzyme resulting in the consumption of 1 μmol of NADH/min (pyruvate kinase) or 2 μmol of ferricyanide/min (succinate dehydrogenase).
[b] Shown is the activity under optimal conditions and substrate for *T. gondii* pyruvate kinase I (1 mM PEP, 1 mM ADP,10 mM $MgSO_4$, 100 mM KCl_2, pH 7.0).
[c] Shown is the activity under optimal conditions and substrate for *T. gondii* pyruvate kinase II (1 mM PEP, 0.5 mM GDP, 25.5 mM $MgCl_2$, pH 8.5).
[d] SDH means succinate dehydrogenase.

SignalP, and ChloroP were used to predict the presence of signals in N-terminal 357 amino acids (Fig. 5). SignalP 3.0 (21) with 100 truncation max residues was used to predict the presence of canonical secretory signal peptide (SP) or anchor (SA) in translation products from five possible start codons (Fig. 5, *ocher*). Although SignalP-NN, the neural networks based algorithm, predicted a weak SP cleavage site between aa 92 and 93 for the 1st Met protein product, SignalP-HMM (41), the hidden Markov model algorithm, highly favors SA ($p = 0.995$). The same prediction was observed for the 2ndMet product. The Kyte-Doolittle hydrophobicity profile showed the presence of a strong hydrophobic stretch between aa ~75 and 92 corresponding the prediction of SignalP (Fig. 5*B*). ChloroP (23) predicted possible plastid transit peptides (pTPs) for translation products from the 1st, 3rd, and 5th Met (Fig. 5, *green*). The predicted pTP cleavage sites for the 1st, 3rd, and 5th Met products are between aa 69 and 70, aa 159 and 160, and aa 309 and 310, respectively (note that amino acid positions are counted from the position of 1st Met). TargetP (20) predicted the presence of mitochondrial targeting peptides (mTPs) for translation products from 3rd, 4th, and 5th Met (Fig. 5, *magenta*). The predicted mTP cleavage sites are between aa 140 and 141 for the 3rd and 4th Met products and aa 316 to 317 for the 5th Met product. Summary of the possible signal sequences for various protein products is shown in Fig. 5*C*.

To determine whether the N-terminal unconserved region of *Tg*PyKII can function as a dual targeting signal to the mitochondrion and the apicoplast, YFP-HA was fused to the N-terminal 357 aa of *Tg*PyKII (*Tg*PyKII1stM-(1–357)-YFP-HA) and expressed in tachyzoites (Fig. 6*A*). YFP labeling co-localizes to both the apicoplast (Fig. 5*A*, *blue*) and the mitochondrion (Fig. 5*A*, *red*), suggesting that this region is responsible for proper localization of *Tg*PyKII. Because this N-terminal extension contains five possible start codons, the dual targeting of *Tg*PyKII1stM-(1–357)-YFP-HA could result from one protein targeted to both organelles or two proteins targeted to each individual organelle. To answer this, we fused YFP-HA to N-terminal unconserved regions starting from downstream possible start codons (at aa positions 19 for 2nd Met, 93 for 3rd Met, 122 for 4th Met, and 293 for 5th Met) and expressed in tachyzoites. YFP labeling of *Tg*PyKII2ndM-(19–357)-YFP-HA (Fig. 6*B*) and *Tg*PyKII3rdM-(93–357)-YFP-HA (Fig. 6*C*) is localized only to the mitochondrion, whereas that of *Tg*PyKII4thM-(122–357)-YFP-HA and *Tg*PyKII5thM-(293–357)-YFP-HA is localized to cytosol (data not shown). These results suggest that the dual targeting of *Tg*PyKII-1stM-(1–357)-YFP-HA could result from one protein product (*i.e.* 1st Met product targeted to both organelles) or two protein products (*i.e.* 1st Met product targeted to the apicoplast and either 2nd Met or 3rd Met product targeted to the mitochondrion). To determine whether there are one or two products responsible for the dual targeting, we performed site-directed mutagenesis changing 2nd Met or 3rd Met to Ala in *Tg*PyKII1stM-(1–357)-YFP-HA construct and expressed them in tachyzoites. Although *Tg*PyKII[2ndM19A]-YFP-HA targets YFP-HA to the apicoplast and the mitochondrion (Fig. 7*A*), *Tg*PyKII[3rdM93A]-YFP-HA targeted only to the apicoplast (Fig. 7*B*). These results suggest that two protein products are responsible for dual targeting, 1st Met product for the apicoplast and the 3rd Met product for the mitochondrion.

DISCUSSION

We characterized a novel pyruvate kinase isozyme in *T. gondii*, *Tg*PyKII, with unique enzymatic properties. pH optimum for *Tg*PyKII activity is at 8.5, and more than 80% of the maximal activity was observed even at pH 9.0, more alkalinic than the pH optima reported for any other pyruvate kinases (5.5–8.0) (42,

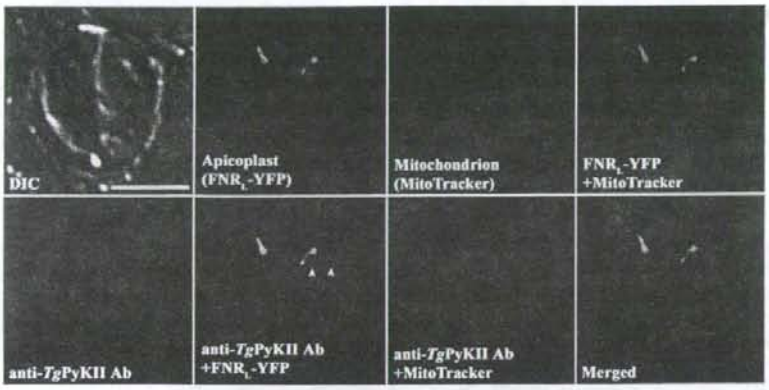

FIGURE 4. **Apicoplast and mitochondrial localization of native *Tg*PyKII in *T. gondii* tachyzoite.** Parasites stably expressing p*tub*FNR$_L$-YFP-HA (labeling apicoplast, *green*) were stained with MitoTracker Red CMXRos (*red*) and anti-*Tg*PyKII antibody (*blue*). Note that in addition to apicoplast and mitochondrion, *Tg*PyKII antibody localizes to apical ER (*arrowheads*) that may indicate a possible exit site of *Tg*PyKII from ER. *Scale bar*, 5 μm. *DIC*, differential interference contrast.

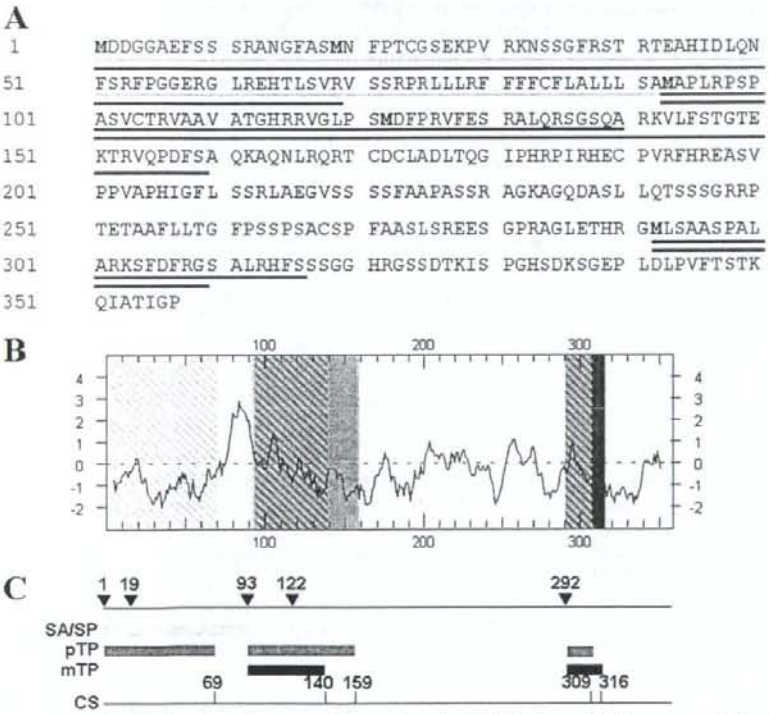

FIGURE 5. **Signal prediction of the N-terminal extension of *Tg*PyKII in *T. gondii*.** *A*, N-terminal 357 amino acid sequence of *Tg*PyKII. Methionines are highlighted in *red*. *Colored underlines* are location of predicted signals (see below for color codes). *B*, Kyte-Doolittle hydrophobicity plot of the N-terminal extension of *Tg*PyKII showing a strong hydrophobic stretch between aa 75 and 92. *Color-shaded* regions are location of predicted signals (see below for color codes). Colors are *hatched* in regions where signals are overlapped. *C*, summary of predicted signals. *Inverted black triangles* indicate the location of each methionine with amino acid position listed above. The *numbers* above the *tick mark* indicate the amino acid position before the predicted signal cleavage sites. *Colored boxes* are location of predicted signals. Predicted SA/SP, *ocher*; predicted plastid transit peptide (pTP), *green*; predicted mitochondrion targeting peptide (mTP), *magenta*; *CS*, cleavage site.

43). Although the actual physiological pH value of the apicoplast or the mitochondrion in *T. gondii* is still unknown, several enzymes localized in the apicoplast in *P. falciparum* (44), plastid in barley roots (45), or mitochondrion in yeast (46) and *Arabidopsis thaliana* (47) have alkaline pH optima like *Tg*PyKII. It is also possible, however, the maximal activity of *Tg*PyKII may not be necessary in parasite survival.

Although ADP is generally considered as the phosphate recipient of pyruvate kinase in glycolysis, pyruvate kinase activity is relatively nonspecific in its utilization of purine and pyrimidine nucleotide substrates (48). Some bacterial pyruvate kinases prefer GDP over ADP (5, 49, 50), but their k_{cat}/K_m (or V_{max}/K_m) ratio for GDP is only 10–20-fold higher than that for ADP. However, in case of *Tg*PyKII, GDP is preferred over ADP as a phosphate recipient with 377-fold higher k_{cat}/K_m (or V_{max}/K_m) ratio, suggesting GDP as a sole phosphate recipient.

Pyruvate kinases are generally activated by sugar phosphates and bind PEP allosterically (51). Albeit fructose 1,6-diphosphate is a typical allosteric activator, some pyruvate kinases use other activators such as fructose 2,6-diphosphate (52) in trypanosomatid protozoans and glucose 6-phosphate in *Eimeria tenella* (53), *Mycobacterium smegmatis* (54), *Strepotcoccus mutans* (49), and *Tg*PyKI (11). Our study shows that *Tg*PyKII is not activated by fructose 1,6-diphosphate and other known activators for pyruvate kinase such as sugar phosphates, and consistently, it does not show allosteric binding to PEP. Thus *Tg*PyKII does not seem to have regulatory properties like as *Tg*PyKI.

Pyruvate kinase can be classified by the requirement for a monovalent cation. Structural analysis (55), point mutation analysis (38, 39), and phylogenetic analysis (40) suggest that (Thr^{113} and Glu^{117}) and (Leu/Ile^{113} and Ser/Lys^{117}) (numbers in *F. catus* pyruvate kinase) are responsible for monovalent cation dependence and independence, respectively. Monovalent cation-independent isozymes (type II) exist in prokaryotes like actinobacteria, cyanobacteria, and proteobacteria, whereas monovalent cation-dependent isozymes (type I) exist in mammals, plants, and fungi (Fig. 2). In prokaryotes, *Clostridium perfringens*, *Leptospira interrogans*,

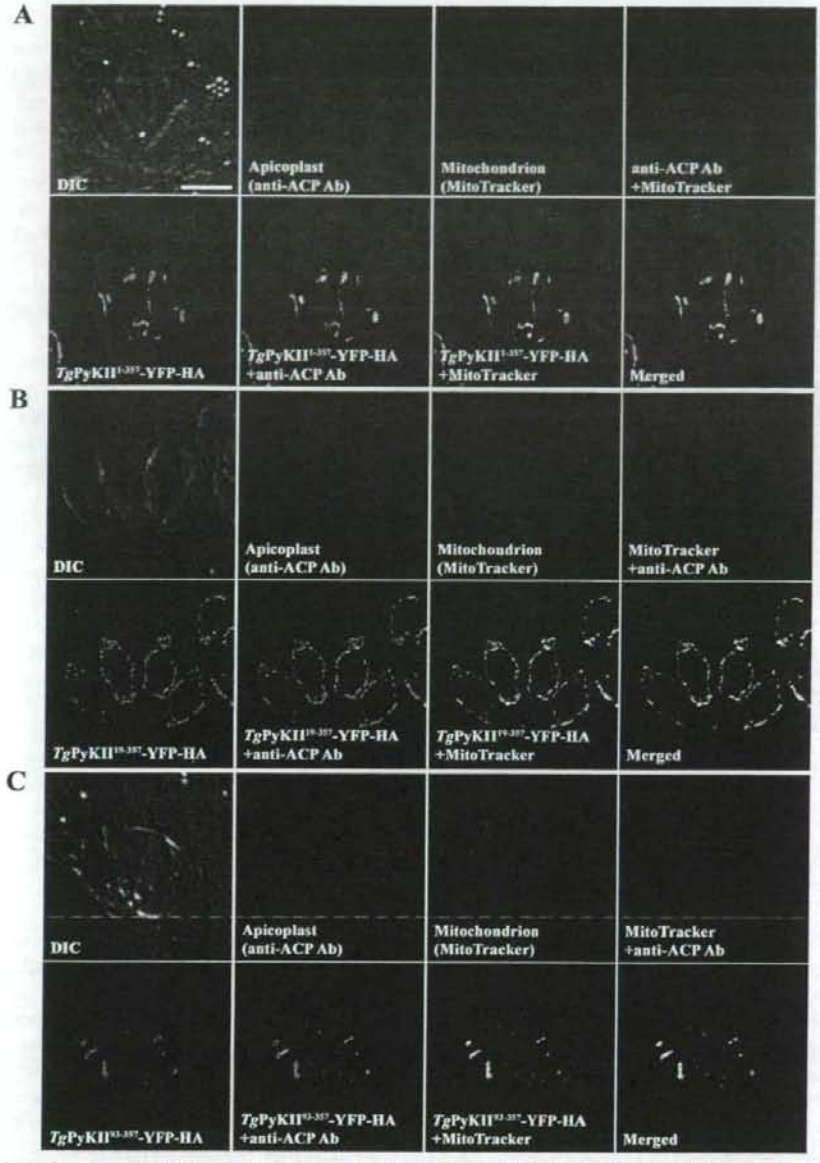

FIGURE 6. **Localization of *Tg*PyKII1stM-(1–357)-YFP-HA, *Tg*PyKII2ndM-(19–357)-YFP-HA, and *Tg*PyKII3rdM-(93–357)-YFP-HA.** Parasites were transfected with *Tg*PyKII1stM-(1–357)-YFP-HA (*A*), *Tg*PyKII2ndM-(19–357)-YFP-HA (*B*), or *Tg*PyKII3rdM-(93–357)-YFP-HA (*C*) under tubulin (in these panels) or dihydrofolate reductase (not shown) promoters and labeled with MitoTracker Red CMXRos (labeling mitochondrion, *red*) and anti-ACP antibody (labeling apicoplast, *blue*). The same phenotype was observed for different promoters. *Scale bar*, 5 μm. *DIC*, differential interference contrast.

E. coli, *Vibrio cholerae*, and *Salmonella typhimurium* possess both types. In eukaryotes, so far only apicomplexan parasites, *T. gondii* (in this study), *P. falciparum* (56), *Theileria annulata* (contig 1823 and contig13), and *T. parva* (529.m04777 and 529.m0471) possess both types. Phylogenetic analysis shows that Apicomplexan type I pyruvate kinase clusters with plants and apicomplexan type II pyruvate kinase with proteobacteria (Fig. 2), suggesting that monovalent cation-independent isozymes (type II) in apicomplexan parasites are of proteobacterial origin and obtained by horizontal gene transfer (Fig. 2). *Neospora caninum* possibly contains the proteobacteria-like pyruvate kinase isozyme (contig5134), but the full sequence has not been determined. The proteobacteria-like pyruvate kinase isozyme is not found in the complete genome sequence data base of *C. parvum*, which possesses a reduced mitochondria (mitome) but lacks the apicoplast. Genome sequencing of *Eimeria tenella* has not been completed at this time.

Another striking feature of *Tg*PyKII is its dual localization to the apicoplast and mitochondrion as there is no documented evidence of a pyruvate kinase present in the mitochondrion in any other organism. In plants, although proteins are normally transported to chloroplasts or mitochondria from cytoplasm using organelle-specific N-terminal targeting signals, pTP or mTP, respectively, proteins can be dually targeted to both organelles by two types of signals as follows: (i) a twin presequence from alternative transcription start, alternative translation start, or alternative exons results in two proteins, one targeted to the chloroplast and the other to the mitochondrion; and (ii) an ambiguous presequence results in one protein targeted to both organelles (57). In *T. gondii*, although mitochondrial proteins use a classical mTP, proteins are targeted to the apicoplast, a secondary endosymbiotic plastid, using a unique N-terminal bipartite signal consisting of a secretory signal peptide (SP) followed by pTP (17, 58). Yet recently, a superoxide dismutase (*Tg*SOD2) having a typical apicoplast bipartite signal is reported to localize to both apicoplast and mitochondrion as a single gene product (59). In this study, we showed that *Tg*PyKII possesses an N-terminal extension, which contains five possible start codons and probable SA/SP, pTP, and mTP (Fig. 5). Using fluorescent reporter fused to N-terminal 357 aa from the 1st Met (*Tg*PyKII1stM-(1–357)-YFP-HA), we prove that this region is responsible for localization to the apicoplast and the mitochondrion. Fluorescent fusions from 2nd and 3rd Met result in localization to the mito-

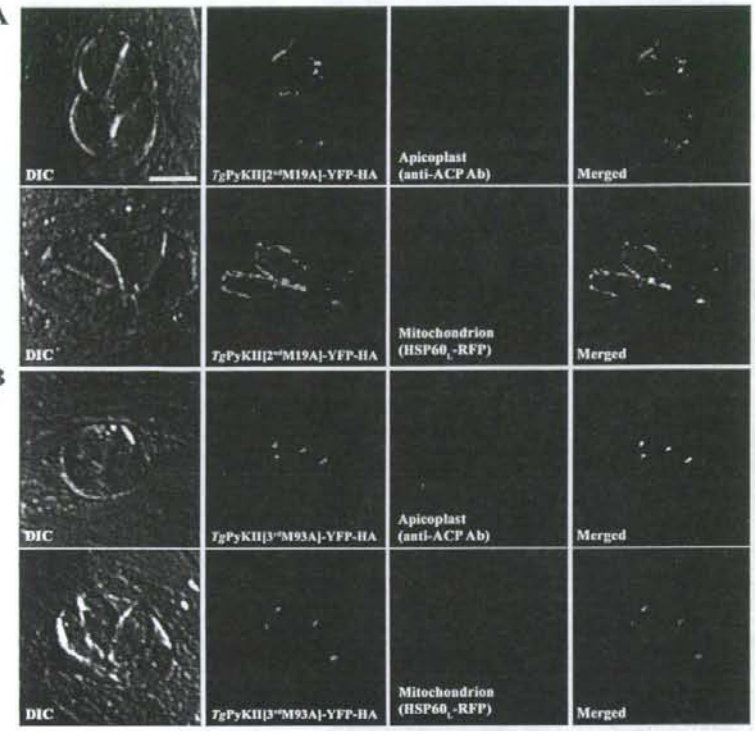

FIGURE 7. **Localization of *Tg*PyKII[2ndM19A]-YFP-HA and *Tg*PyKII[3rdM93A]-YFP-HA.** *A*, localization of *Tg*PyKII[2ndM19A]-YFP-HA. *Top panels*, wild type RH parasites transfected with p*minTg*PyKII[2ndM19A]-YFP-HA (*green*) and labeled with anti-ACP antibody (labeling apicoplast, *red*). *Bottom panels*, RH parasites stably expressing HSP60$_L$-RFP (labeling mitochondrion, *red*) transfected with p*minTg*PyKII[2ndM19A]-YFP-HA (*green*). *B*, localization of *Tg*PyKII[3rdM93A]-YFP-HA. *Top panels*, wild type RH parasites transfected with p*minTg*PyKII[3rdM93A]-YFP-HA (*green*) and labeled with anti-ACP antibody (labeling apicoplast, *red*). *Bottom panels*, RH parasites stably expressing HSP60$_L$-RFP (labeling mitochondrion, *red*) transfected with p*minTg*PyKII[3rdM93A]-YFP-HA (*green*). The same phenotype was observed for constructs under tubulin promoter. *Scale bar*, 5 μm. *DIC*, differential interference contrast.

chondrion only, suggesting that 1st Met product is responsible for apicoplast localization. *Tg*PyKII was predicted to have an SA/SP (with higher probability for SA) from aa 1 to 92 (Fig. 5, *ocher*) because of an unusual hydrophobic region rich in leucine and phenylalanine between aa 75 and 92. However, *Tg*PyKII2ndM-(19–357)-YFP-HA, despite containing this hydrophobic region, does not localize to the apicoplast, suggesting that 18 aa between the 1st and 2nd Met is necessary for proper translocation into the ER and thus the apicoplast. Site-directed mutagenesis analysis showed that 3rd Met translation product, not 2nd Met, in the N-terminal extension of *Tg*PyKII is responsible for the localization to the mitochondrion, consistent with the presence of mTP from 3rd Met (Fig. 5, *magenta*). Thus, unlike *Tg*SOD2, two translation products are responsible for dual localization of *Tg*PyKII, 1st Met product for the apicoplast and 3rd Met product for the mitochondrion. Further characterization of signals and signal cleavage sites has currently been carried out.

Type I monovalent cation-dependent isozymes in the apicomplexa lack an N-terminal extension, suggesting that, as in *Tg*PyKI, they localize in the cytosol. On the other hand, type II monovalent cation-independent isozymes with proteobacterial origin found in *P. falciparum*, *T. annulata*, and *T. parva* possess an N-terminal extension containing a typical bipartite apicoplast targeting signal. *P. falciparum* PyKII (AAN35560) does not have any internal methionines and was shown to localize only to the apicoplast by immunostaining using native antibody.[6] *T. parva* PyKII (529.m04771) has internal methionines and could be dual-localized like as *Tg*PyKII.

Although plant isozyme in plastids (60, 61) is a noncytosolic pyruvate kinase that functions in the glycolysis (62), noncytosolic pyruvate kinase found in the apicomplexan parasites may be involved in a unique metabolic pathway other than glycolysis, in which cytosolic pyruvate kinase plays a regulatory role. A plastidic sugar phosphate transporter was shown to localize to the apicoplast of *T. gondii* (16), which may suggest that triose sugars such as PEP could be transported from the cytosol to the apicoplast. Pyruvate dehydrogenase complex (59, 63, 64), enzymes in type II fatty acid synthesis (65, 66), and 1-deoxy-D-xylulose 5-phosphate synthesis (67) are localized in the apicoplast in *T. gondii*. Thus, in the apicoplast, *Tg*PyKII may function in supplying acetyl Co-A in cooperation with pyruvate dehydrogenase complex for fatty acid as well as 1-deoxy-D-xylulose 5-phosphate syntheses, as suggested in *P. falciparum* (68). Although *T. parva* does not possess FAS pathway in the apicoplast, PyKII in *T. parva* may contribute to the 1-deoxy-D-xylulose 5-phosphate pathway (69). The unique GTP supply role of *Tg*PyKII may contribute to provide an energy source for protein synthesis and a substrate for RNA synthesis in the apicoplast that has its own DNA (70).

To date, pyruvate kinase has not been identified in the mitochondria of any organism. As the substrate PEP can be provided from gluconeogenesis pathway through mitochondrial PEP carboxykinase (NCBI ID BAC02911), this unusual "short cut" might contribute to the rapid switching from gluconeogenesis to the oxidative phosphorylation. However, the fate of the product pyruvate is currently unknown, as pyruvate dehydrogenase complex does not localize in the mitochondrion (59, 64), whereas *T. gondii* tricarboxylic acid cycle is functional in the tachyzoite stage (71–73). The metabolic pathway connecting pyruvate with tricarboxylic acid cycle in the mitochondria in

[6] T. Maeda, T. Saito, O. Harb, D. S. Roos, A. Takeo, H. Suzuki, T. Tsuboi, T. Takeuchi, and T. Asai, unpublished data.

the apicomplexan parasites has been the unsolved question (34, 59, 63, 64). Although currently available data from biochemical and bioinformatics analyses do not provide explicit explanation for the role of *Tg*PyKII in the *T. gondii* mitochondrion, as the dual targeting to the apicoplast and mitochondrion can occur in previously unpredictable mechanisms in *T. gondii* (59 and in this study), further studies on experimental protein targeting may reconstruct metabolic pathways, and detailed information about the intraorganelle milieu will elucidate the physiological role of *Tg*PyKII in the mitochondrion.

REFERENCES

1. Dubey, J. P. (1993) in *Parasitic Protozoa* (Kreier, J. P., ed) pp. 5–56, Academic Press, San Diego
2. Fulton, J. D., and Spooner, D. F. (1960) *Exp. Parasitol.* **9,** 293–301
3. Boyer, P. D. (1962) in *The Enzymes* (Boyer, P. D., Lardy, H., and Myrback, K., eds) 2nd Ed., pp. 95–113, Academic Press, New York
4. Valentini, G., Chiarelli, L., Fortin, R., Speranza, M. L., Galizzi, A., and Mattevi, A. (2000) *J. Biol. Chem.* **275,** 18145–18152
5. Waygood, E. B., and Sanwal, B. D. (1974) *J. Biol. Chem.* **249,** 265–274
6. Waygood, E. B., Rayman, M. K., and Sanwal, B. D. (1975) *Can. J. Biochem.* **53,** 444–454
7. Plaxton, W. C. (1996) *Annu. Rev. Plant Physiol. Plant Mol. Biol.* **47,** 185–214
8. Saito, T., Maeda, T., Nakazawa, M., Takeuchi, T., Nozaki, T., and Asai, T. (2002) *Int. J. Parasitol.* **32,** 961–967
9. Peng, Z. Y., and Mansour, T. E. (1992) *Mol. Biochem. Parasitol.* **54,** 223–230
10. Denton, H., Roberts, C. W., Alexander, J., Thong, K. W., and Coombs, G. H. (1996) *FEMS Microbiol. Lett.* **137,** 103–108
11. Maeda, T., Saito, T., Oguchi, Y., Nakazawa, M., Takeuchi, T., and Asai, T. (2003) *Parasitol. Res.* **89,** 259–265
12. Bahl, A., Brunk, B., Crabtree, J., Fraunholz, M. J., Gajria, B., Grant, G. R., Ginsburg, H., Gupta, D., Kissinger, J. C., Labo, P., Li, L., Mailman, M. D., Milgram, A. J., Pearson, D. S., Roos, D. S., Schug, J., Stoeckert, C. J., Jr., and Whetzel, P. (2003) *Nucleic Acids Res.* **31,** 212–215
13. Hoffman, S. L., Subramanian, G. M., Collins, F. H., and Venter, J. C. (2002) *Nature* **415,** 702–709
14. Roos, D. S., Donald, R. G., Morrissette, N. S., and Moulton, A. L. (1994) *Methods Cell Biol.* **45,** 27–63
15. Asai, T., and Suzuki, Y. (1990) *FEMS Microbiol. Lett.* **60,** 89–92
16. Nishi, M. (2006) *Cell-cycle Regulation of Organelle Biogenesis and Apicoplast Protein Trafficking in Toxoplasma gondii.* Ph.D. thesis, University of Pennsylvania
17. Waller, R. F., Keeling, P. J., Donald, R. G., Striepen, B., Handman, E., Lang-Unnasch, N., Cowman, A. F., Besra, G. S., Roos, D. S., and McFadden, G. I. (1998) *Proc. Natl. Acad. Sci. U. S. A.* **95,** 12352–12357
18. Kissinger, J. C., Gajria, B., Li, L., Paulsen, I. T., and Roos, D. S. (2003) *Nucleic Acids Res.* **31,** 234–236
19. Hulo, N., Bairoch, A., Bulliard, V., Cerutti, L., De Castro, E., Langendijk-Genevaux, P. S., Pagni, M., and Sigrist, C. J. (2006) *Nucleic Acids Res.* **34,** D227–D230
20. Emanuelsson, O., Nielsen, H., Brunak, S., and von Heijne, G. (2000) *J. Mol. Biol.* **300,** 1005–1016
21. Nielsen, H., Engelbrecht, J., Brunak, S., and von Heijne, G. (1997) *Protein Eng.* **10,** 1–6
22. Bendtsen, J. D., Nielsen, H., von Heijne, G., and Brunak, S. (2004) *J. Mol. Biol.* **340,** 783–795
23. Emanuelsson, O., Nielsen, H., and von Heijne, G. (1999) *Protein Sci.* **8,** 978–984
24. Kyte, J., and Doolittle, R. F. (1982) *J. Mol. Biol.* **157,** 105–132
25. Chen, F., Mackey, A. J., Stoeckert, C. J., Jr., and Roos, D. S. (2006) *Nucleic Acids Res.* **34,** D363–D368
26. Li, L., Stoeckert, C. J., Jr., and Roos, D. S. (2003) *Genome Res.* **13,** 2178–2189
27. Thompson, J. D., Gibson, T. J., Plewniak, F., Jeanmougin, F., and Higgins, D. G. (1997) *Nucleic Acids Res.* **25,** 4876–4882
28. Felsenstein, J. (1989) *Cladistics* **5,** 164–166
29. Schmidt, H. A., Strimmer, K., Vingron, M., and von Haeseler, A. (2002) *Bioinformatics (Oxf.)* **18,** 502–504
30. Huelsenbeck, J. P., and Ronquist, F. (2001) *Bioinformatics (Oxf.)* **17,** 754–755
31. Ronquist, F., and Huelsenbeck, J. P. (2003) *Bioinformatics (Oxf.)* **19,** 1572–1574
32. Kahn, A., and Marie, J. (1982) *Methods Enzymol.* **90,** 131–140
33. Sibley, L. D., Niesman, I. R., Asai, T., and Takeuchi, T. (1994) *Exp. Parasitol.* **79,** 301–311
34. van Dooren, G. G., Stimmler, L. M., and McFadden, G. I. (2006) *FEMS Microbiol. Rev.* **30,** 596–630
35. Muirhead, H., Clayden, D. A., Barford, D., Lorimer, C. G., Fothergill-Gilmore, L. A., Schiltz, E., and Schmitt, W. (1986) *EMBO J.* **5,** 475–481
36. Mattevi, A., Valentini, G., Rizzi, M., Speranza, M. L., Bolognesi, M., and Coda, A. (1995) *Structure (Lond.)* **3,** 729–741
37. Rigden, D. J., Phillips, S. E., Michels, P. A., and Fothergill-Gilmore, L. A. (1999) *J. Mol. Biol.* **291,** 615–635
38. Laughlin, L. T., and Reed, G. H. (1997) *Arch. Biochem. Biophys.* **348,** 262–267
39. Jurica, M. S., Mesecar, A., Heath, P. J., Shi, W., Nowak, T., and Stoddard, B. L. (1998) *Structure (Lond.)* **6,** 195–210
40. Oria-Hernandez, J., Riveros-Rosas, H., and Ramirez-Silva, L. (2006) *J. Biol. Chem.* **281,** 30717–30724
41. Krogh, A., and Nielsen, H. (1998) in *Proceedings of the Sixth International Conference on Intelligent Systems for Molecular Biology (ISMB 6), Menlo Park, June 28–July 1, 1998,* pp. 122–130, AAAI Press, Menlo Park, CA
42. Saavedra, E., Olivos, A., Encalada, R., and Moreno-Sanchez, R. (2004) *Exp. Parasitol.* **106,** 11–21
43. Hattori, J., Baum, B. R., McHugh, S. G., Blakeley, S. D., Dennis, D. T., and Miki, B. L. (1995) *Biochem. Syst. Ecol.* **23,** 773–780
44. Dhanasekaran, S., Chandra, N. R., Chandrasekhar Sagar, B. K., Rangarajan, P. N., and Padmanaban, G. (2004) *J. Biol. Chem.* **279,** 6934–6942
45. Esposito, S., Carfagna, S., Massaro, G., Vona, V., and Di Martino Rigano, V. (2001) *Planta* **212,** 627–634
46. Jault, J. M., Di Pietro, A., Falson, P., and Gautheron, D. C. (1991) *J. Biol. Chem.* **266,** 8073–8078
47. Olejnik, K., Murcha, M. W., Whelan, J., and Kraszewska, E. (2007) *FEBS J.* **274,** 4877–4885
48. Plowman, K. M., and Krall, A. R. (1965) *Biochemistry* **4,** 2809–2814
49. Abbe, K., and Yamada, T. (1982) *J. Bacteriol.* **149,** 299–305
50. Crow, V. L., and Pritchard, G. G. (1982) *Methods Enzymol.* **90,** 165–170
51. Munoz, M. E., and Ponce, E. (2003) *Comp. Biochem. Physiol. B. Biochem. Mol. Biol.* **135,** 197–218
52. van Schaftingen, E., Vandercammen, A., Detheux, M., and Davies, D. R. (1992) *Adv. Enzyme Regul.* **32,** 133–148
53. Denton, H., Brown, S. M., Roberts, C. W., Alexander, J., McDonald, V., Thong, K. W., and Coombs, G. H. (1996) *Mol. Biochem. Parasitol.* **76,** 23–29
54. Kapoor, R., and Venkitasubramanian, T. A. (1981) *Biochem. J.* **193,** 435–440
55. Larsen, T. M., Laughlin, L. T., Holden, H. M., Rayment, I., and Reed, G. H. (1994) *Biochemistry* **33,** 6301–6309
56. Gardner, M. J., Hall, N., Fung, E., White, O., Berriman, M., Hyman, R. W., Carlton, J. M., Pain, A., Nelson, K. E., Bowman, S., Paulsen, I. T., James, K., Eisen, J. A., Rutherford, K., Salzberg, S. L., Craig, A., Kyes, S., Chan, M. S., Nene, V., Shallom, S. J., Suh, B., Peterson, J., Angiuoli, S., Pertea, M., Allen, J., Selengut, J., Haft, D., Mather, M. W., Vaidya, A. B., Martin, D. M., Fairlamb, A. H., Fraunholz, M. J., Roos, D. S., Ralph, S. A., McFadden, G. I., Cummings, L. M., Subramanian, G. M., Mungall, C., Venter, J. C., Carucci, D. J., Hoffman, S. L., Newbold, C., Davis, R. W., Fraser, C. M., and Barrell, B. (2002) *Nature* **419,** 498–511
57. Peeters, N., and Small, I. (2001) *Biochim. Biophys. Acta* **1541,** 54–63
58. Roos, D. S., Crawford, M. J., Donald, R. G., Kissinger, J. C., Klimczak, L. J., and Striepen, B. (1999) *Curr. Opin. Microbiol.* **2,** 426–432
59. Pino, P., Foth, B. J., Kwok, L. Y., Sheiner, L., Schepers, R., Soldati, T., and Soldati-Favre, D. (2007) *Plos Pathog.* **3,** e115